Tks5 interactome reveals ER-associated machinery translation in invadosomes.

Léa Normand[1], Benjamin Bonnard[1], Margaux Sala[1], Sylvaine Di-Tommaso[1,2], Cyril Dourthe[1,2], Anne-Aurélie Raymond[1,2], Jean-William Dupuy[2,3], Luc Mercier[4], Jacky G. Goetz[4], Violaine Moreau[1], Elodie Henriet[1#] and Frédéric Saltel[1,2#].

[1]University of Bordeaux, Inserm, UMR1312, BRIC, BoRdeaux Institute of onCology, 146 Rue Léo Saignat, Bordeaux, F-33000, France.

[2]University of Bordeaux, CNRS, INSERM, TBM-Core, US5, UAR 3427, OncoProt, F-33000 Bordeaux, France Labeled LNCC.

[3]University of Bordeaux, Bordeaux Proteome, F-33000 Bordeaux, France.

[4]Inserm U1109, MN3T, Strasbourg, France ; Université de Strasbourg, Strasbourg, France ; LabEx Medalis, Université de Strasbourg, Strasbourg, France ; Fédération de Médecine Translationnelle de Strasbourg (FMTS), Strasbourg, F-67000, France.

[#] These authors contributed equally to this work.

Corresponding author: frederic.saltel@inserm.fr

Summary

Invadosomes are invasive F-actin structures exhibiting different organizations that degrade the extracellular matrix. The study uses their universal marker, Tks5, to provide new data about invadosome molecular composition and reveal the role of ER-associated translation machinery in invadosome formation and function.

Abbreviations

CHX: cycloheximide

ECM: extracellular matrix

EIF4B: eukaryotic translation initiation factor 4B

ER: endoplasmic reticulum

RPS6: ribosomal subunit S6

Abstract:

The ability to progress and invade through the extracellular matrix is a characteristic shared by both normal and cancer cells through the formation of structures called invadosomes. These invadosomes are plastic and dynamic structures that can adopt different organizations depending on the cell types and the environment such as rosettes, dots or linear invadosomes. In this study, we used the specific invadosome marker Tks5, to identify common features in these different organizations. Tks5 immunoprecipitation coupled with mass spectrometry analysis allowed us to identify common proteins in these different models. We identified elements of the translation machinery, in particular the EIF4B protein, but also endoplasmic reticulum (ER) proteins as part of the invadosome structure. Providing new data on invadosome molecular composition through Tks5 interactome, we identified that ER-associated translation machinery is recruited to invadosome formation, persistence and function in all types of invadosomes.

Keywords: cancer, Tks5, invadosomes, ER, translation

Introduction

The ability to progress and invade through the surrounding environment is a characteristic shared by both normal and tumor cells. Extracellular matrix (ECM) breaching such as basement membrane or fibrillar collagen rich matrices is needed in physiological conditions such as embryogenesis or wound healing but is also required at the early stages of the metastatic cascade. During metastasis, cells will invade their surrounding matrix thanks to invadosomes. Invadosomes are dynamic actin-based structures that allow cells to interact and remodel the ECM through the recruitment of metalloproteinases [1,2]. Invadosome formation has been shown to depend on different factors such as soluble factors like growth factors [3–5] or the mechanical properties [6,7] and composition of the ECM [8]. These structures, classified as podosomes and invadopodia, respectively in normal cells and tumor cells, can adopt different organizations such as rosettes, aggregates or dots [6]. These plastic and dynamic structures are able to sense and adapt to their environment composition. Laminin can promote the formation of dots [9,10], while fibrillar type I collagen matrix leads to a re-organization along the fibers forming linear invadosomes [9,11] demonstrating a microenvironment-induced remodeling. This morphological plasticity is associated with a variation of the molecular composition of the structures: podosomes present a ring of adhesive proteins which is absent in invadopodia or linear invadosomes [11]. While podosomes and invadopodia are integrin-dependent structures, linear invadosome formation specifically depends on the discoidin domain receptor 1 (DDR1) [9,12]. On the other hand, actin-binding proteins like cortactin, the Arp2/3 complex, the neuronal Wiskott-Aldrich syndrome protein (N-WASP) and the GTPase Cdc42 are shared by all invadosome structures, but are also present in other actin structures [13–15]. However, the Tks5 scaffolding protein appears as a specific and common marker to all types of invadosomes[15]. Indeed, this protein is enriched in invadosomes but not in focal adhesion, filopodia, membrane ruffle or lamellipodia[16]. Tks5, a Src substrate protein, is required for invadosome formation [16]. Tks5 was discovered by Lock et *al.* in 1998 and is part of the p47 family [17]. It contains two major domains, the PX one that allows anchoring to the membrane, and the SH3 domain that allows protein-protein interaction. In addition to its major role in invadosome formation, Tks5 is also involved in cell division in bladder cancer and in cell proliferation via its action during the G1 phase of the cell cycle [18,19]. Tks5 belongs to a family containing also the Tsk4 protein involved in ECM degradation, only in podosomes, while Tks5 is involved in all invadosome formation [20].

Even if several studies over the last few years have aimed at better defining molecular composition involved in invadosome formation[21,22], the common or specific markers for each structures in regard to their plasticity need to be investigated.

The aim of this article was to identify new and common molecular components present in all types of invadosome forms, namely rosettes, dots and linear invadosomes. To do so, we performed Tks5 interactome in different invadosomes models. We used two cellular models, NIH3T3-Src and a melanoma cancer cell line A431, in two ECM contexts to generate rosettes, dots and linear invadosomes.

We identified 88 proteins commonly enriched in Tks5 interactome from four different types of invadosomes. While several identified proteins were already known to be involved in the formation or function of invadosomes (CD44, cortactin, ADAM15 or MMP14), we highlighted 54 new proteins not described to be involved into invadosome formation and/or function. Among these proteins, a large proportion was related to translation machinery confirming data obtained in a previous study[21]. We identified the eukaryotic translation initiation factor 4B (EIF4B) into invadosomes. We confirmed that translation and EIF4B are involved in the matrix degradation activity. Furthermore, we showed that the presence of endoplasmic reticulum (ER) proteins is required for invadosome persistence. These findings provide a better understanding of the invadosome regulation through the ER-associated translation machinery.

Results

Invadosomes variability and plasticity.

In order to compare the different invadosome structures, we chose two complementary cellular models. The Src-transformed mouse fibroblast NIH-3T3-Src cell line that present podosomes as rosettes when cultured on a gelatin substrate and the A431 human epidermoid carcinoma cell line which form invadopodia as dots (Figure 1a-b). As expected, the fibrillar collagen matrix led to their reorganization as linear invadosomes with a co-localization of F-actin and Tks5 along the collagen fibers in both cell lines (Figure 1a-b). These elements these elements demonstrate the variability and plasticity of invadosomes. Thus, Tks5 is a universal marker of rosettes, dots and linear invadosomes, and is the best candidate to investigate common invadosome features.

Proteomics analysis of Tks5 interactome in invadosomes.

To determine Tks5 interactome in these invadosome types, we transfected NIH-3T3-Src and A431 cells with GFP-tagged Tks5 encoding plasmid. As expected, GFP-Tks5 colocalizes with endogenous Tks5 in all types of invadosomes (Figure 2a). We realized immunoprecipitation against GFP in both cell lines on plastic and type I collagen conditions (Supp Figure 1a). Tks5 interactome was then assessed by LC-MS/MS mass spectrometry and the results are show in the Supplemental Table 1.

We first determined the specific molecular signature associated with each invadosome organization. We commonly identified an enrichment in mitochondrial, endoplasmic reticulum (ER) and Golgi proteins (Supp Figure 1b-g). The gene set enrichment analysis (GSEA) performed on Tks5 interactome from linear invadosomes (A431 and NIH-3T3-Src cells) showed an enrichment for cell adhesion proteins such as CD34 and TSPAN6 absent in other invadosome organizations (Supp Figure 1f). These data show that depending on each organization, invadosomes exhibit specific proteins probably involved in their structure or function. Similarly, we also showed specific enrichment of translation proteins although each is organization specific: EIF5A in rosettes, RPS15 in dots or EIF2B4 in linear invadosomes (Supp Figure 1c, e, g).

We performed a comparative analysis with published data regarding proteins associated with Tks5 in 293T cells [22], and also identified cortactin (CTTN), the molecular chaperone Hsp90B1, the elongation factor EEF2 or the beta-actin protein (ACTB) (Supp Figure 2a, left panel).

Similarly, another recent study that used proximity-labelling proteomic assay to identify Tks5 interactome in invadopodia in MDA-MB-231 cells, also identified CTTN, the microtubule-associated protein 4 (MAP4), the reticulon 4 protein (RTN4), the metalloproteinase ADAM15 and the eukaryotic translation initiation factor 4A3 (EIF4A3)[23] (Supp Figure 2a, right panel). Since cortactin is well known to be present in all types of invadosomes, it can be used as a positive control to our approach[24,25].

We then focused on proteins that were common to all invadosomes and identified 88 proteins present in dots, rosettes and linear invadosomes in the two cell types (Figure 2b). Among the 88 common proteins, 34 proteins such as CTTN, LAMP1, ADAM15 or MMP14 were previously identified in literature as components of in invadosomes, validating our mass spectrometry experiment. In order to validate identified proteins known to interact with Tks5[23,26,27], we stained by immunofluorescence the receptor CD44 in all types of invadosomes and confirmed the co-localization of CD44 with Tks5 in all organizations of invadosomes (Figure 2e). Interestingly, the pattern of CD44 is different in rosettes where it colocalize with the actin, in comparison with dots and linear invadosome where CD44 surrounds the actin. Similarly, MAP4 co-localized with Tks5 in dots and linear invadosomes in A431 cells (Supp Figure 2b). These experiments confirm the correct co-localization between Tks5 and the proteins identified in Tks5 interactome by mass spectrometry analysis.

However, a large proportion has never been described to be present in invadosomes such as RPL19, RTN4 or EIF3A (Figure 2c). The GSEA performed on the 88 common proteins showed an enrichment in translation signaling (52% of total proteins) with an enrichment of RNA binding and structural constituent of ribosomes proteins (Figure 2d), including determinant elements of translation machinery such as RPL19, EIF4B or RPS6 (Supp Figure 2c). RPS6 is a component of the 40S subunit of the ribosome that allows the reading of mRNA[28]. EIF4B, on the other hand, is a translation factor that is part of the pre-initiation complex[29]. This complex, in association with the 40S subunit, allows to start mRNA translation. This result confirms the presence of the translation machinery at invadosomes, already identified by our team in NIH-3T3-Src cells using proteomics on laser captured rosette-like invadosomes (Ezzoukhry et *al.)*.

All together these results validate our experimental approach leading to the identification of new Tks5 partners into all types of invadosomes and suggest a link between Tks5 and the translation machinery.

The translation machinery is present in all types of invadosomes.

As we identified the translation machinery as a common feature shared by all the invadosome strucutures, we decided to focus our analysis on these translation proteins. Interestingly, other molecular studies of invadosomes, whether global or linked to Tks5, have identified proteins linked to translation[21–23,30] (Supp Figure 3a). Briefly, Mallawaaratchy et *al.* identified proteins enriched in invadopodia of glioblastoma cells by mass spectrometry, Ezzoukhry et *al.* identified translation proteins enriched in invadosomes by laser microdissection combined with mass spectrometry, Stylli et *al.* identified proteins linked to Tks5 by co-immunoprecipitation and mass spectrometry in dots of 293T cells and Thuault et *al.* identified proteins linked to Tks5 by biotynilation technique in dots of MDA-MB-231. The RPS6 staining and the co-localization with Tks5 validated the presence of ribosomal proteins in all invadosomes (Figures 3a, 3b). We also showed the co-localization of the translational initiation factor, EIF4B, which was previously found enriched in rosettes[21], with Tks5 in all organizations of invadosomes in both cell lines (Figure 3c and 3d). The presence of ribosomal proteins and translation factors in all invadosomes supports the hypothesis on an active translation in these structures.

Involvement of the translation machinery in invadosome function.

In order to investigate the role of translation in all invadosomes formation and matrix degradation activity from both cell lines, we treated A431 and NIH-3T3-Src cells seeded on gelatin or type 1 collagen with the translation inhibitor cycloheximide (CHX) (Supp Figure 3). Our previous study demonstrated that CHX blocked the formation of rosettes in a short time, after one hour of treatment[21]. By using Western Blot and SUrface SEnsing of translation (SUnSET) assay, we first showed that CHX treatment reduced global translation in all conditions (Supp Figure 3b and 3c). We next confirmed that CHX treatment in NIH-3T3-Src model prevented invadosome rosette formation (Figure 4a, 4b) as previously described[21]. No significant differences for dots and linear invadosomes formation was measured by immunofluorescence quantification between CHX and control group (DMSO) (Supp Figure 3d and 3e). However, CHX treatment limited invadosome degradation activity by A431 and NIH-3T3-Src cells on gelatin and collagen matrices (Figure 4c, 4d). These results showed that global translation is involved in degradation capacity of all invadosomes.

As we identified EIF4B in all invadosomes (Figure 2c; Supp Figure 2c), we assessed the role of EIF4B in invadosome degradation activity. By using small interfering RNA (siRNA) strategy we silenced EIF4B expression in both cell lines (Supp Figure 3f) and demonstrated that EIF4B depletion reduced matrix degradation activity in all organizations of invadosomes from both

cell lines (Figure 4e, 4f). These results showed that EIF4B is involved in degradation capacity of all invadosomes.

These data confirm the involvement of the translation and more specifically of the EIF4B protein in the matrix degradation activity of all invadosomes.

Recruitment of ER into invadosome rosettes.

In addition to translation proteins, the mass spectrometry analysis highlighted the presence of ER-related proteins such as RTN4, LRRC59 or RRBP1 in all invadosomes linked with Tks5 (Figure 2c). Ribosomes and ER proteins have previously been identified in the proteome of invadosome rosettes [21]. We thus decided to further investigate the role of the ER in invadosome formation, focusing on rosettes. Comparative analysis, using dataset obtained from Tks5 interactome from NIH-3T3-Src cells harboring rosettes and published rosettes proteome[21], showed an enrichment in ribosomal and translation proteins (Figure 5a). We commonly identified 79 proteins including 39 related to translation proteins (Supp Table 2). Among these 39 proteins, 20 are ribosomal proteins (Supp Table 2) which confirms the presence of ribosomes into invadosome rosettes as observed in Ezzoukhry et al.

In order to assess the involvement of the ER in invadosome formation, we used the rosette model, which is the largest invadosome structure, facilitating analysis and imaging. We used lifeact-mRuby-expressing NIH-3T3-Src cells transfected with KDEL-GFP to detect ER presence. By video microscopy, we showed that the ER was recruited at the level of the rosette in formation and that there was an enrichment of the ER inside the actin core, as previously described in fixed cells[21] (Figure 5b, Video 1). Furthermore, time-lapse imaging revealed that the ER forms “arms” leading to a “ER flow” heading towards the forming rosette then accumulating within the actin core (Figure 5b, Vidéo 1). 3D reconstruction allowed us to visualize the accumulation of the ER within the rosette core (Figure 5c). The transversal sections confirm the enrichment as we can clearly see that the ER arm is inserted within the rosette actin core (Figure 5c). In order to confirm the presence of ER at the level of rosettes, we performed correlative light and electron microscopy (CLEM). Correlation between actin fluorescent images and electron microscopy allowed the identification of ER tubules associated with the rosettes (Figure 5d).

In order to determine the dynamic of ER recruitment during invadosome formation, time-lapse imaging was performed. The analysis revealed that ER recruitment occurs before actin

polymerization and formation of rosette-like invadosomes (Figure 5e, Video 2). In addition, we showed that the maintenance of the structures requires the presence of ER (Figure 5f upper panel, Video 3a) while a drop in ER recruitment is associated with a collapse of the structure (Figure 5f lower panel, Video 3b). 3D reconstruction confirmed that the collapse of the rosette structure is associated with a withdrawal of the ER within the structure with the "ER flow" heading towards the interior of the cell (Figure 5g). These results therefore confirm the presence but also the involvement of the ER in the rosette formation and maintenance over time.

Involvement of ER-associated machinery translation in invadosome formation

As we identified the presence and the determinant role of translation and ER in invadosome formation, we investigated the role of ER-associated translation in invadosome formation and matrix degradation activity. Previously published results showed the involvement of the ER in the formation and function of invadosomes via the involvement of the protrudin protein or by the involvement of the calnexin/erp57 protein complex respectively [31,32]. To determine the role of ER-associated translation in the dynamic of invadosome rosettes formation, we performed a time-lapse experiment with cells treated with CHX to inhibit translation (Figure 6a, Video 4). Translation inhibition led to the collapse of the rosette structure while the ER was still present at the 'previous invadosome site" without re-formation of invadosomes (even if some actin polymerization events were recorded) (Figure 6a, Video 4). This result suggests that ER-associated translation is mandatory for invadosome persistence.

To further characterize the involvement ER-associated translation in invadosome formation, we treated cells with Sec 61 translocon inhibitor (ES1) which blocks the translocation of proteins to the ER. Indeed, Sec61 is a well-described ER marker that allows protein insertion into the ER but also is a key player for ribosomes docking to the ER[33]. Furthermore, Sec61 was identified by our mass spectrometry analysis for A431 cells on plastic and collagen (Supp Table 1). ES1 treatment on A431 and NIH-3T3-Src cells seeded on gelatin or type 1 collagen matrix led to a decreased number of all organizations of invadosomes (Figure 6b). These results therefore suggest that the translation machinery must be adapted somewhat depending on the matrix context. This would explain why the translation machinery is only involved in the degradation function for dots and linear invadosomes while it is involved in the formation and degradation function for rosettes, which are larger structures.

All together, these results demonstrate that the ER-associated translation machinery identified in Tks5 interactome is an essential element to maintain the formation of all types of invadosomes.

Discussion

We provided here a molecular characterization of all types of invadosomes by identifying the interactome of the common and universal invadosome marker Tks5. We used co-immunoprecipitation coupled with mass spectrometry to identify new proteins shared by different invadosome types such as dots, rosettes and linear invadosomes. This strategy allowed us to identify proteins already known in the literature but also to identify new ones. We showed that Tks5 is linked to translation proteins and confirm that translation is involved in the degradation function in all types of invadosomes, including linear invadosomes.

Indeed, we identified 46 translation proteins with some already known in the literature to be involved in invadosome activity such as IGF2BP2 and IGF2BP3 [34–36]. Regarding the other proteins identified and already described in invadosomes, microtubule-associated proteins and especially MAP4 and LAMP1 were described in podosomes [23,26,37] and ITGA5 was described in invadopodia [30]. PTBP1 was also identified in podosomes as participating in their formation[38]. We further demonstrated here that the matrix receptor CD44 which was previously described in podosomes and invadopodia but not in linear invadosomes [27,39] is also a common marker of invadosomes. These known proteins allowed us to serve as quality control for mass spectrometry experiments.

Thanks to mass spectrometry experiments, we were also able to show for the first time the presence of translation proteins in linear invadosomes. We identified the presence of EIF4B and RPS6 proteins in all invadosome organizations. Interestingly, these two proteins are known in the literature to be targeted by the mTOR/ S6K1 pathway. Indeed, S6K1 is be able to directly phosphorylate EIF4B to allow the recruitment of EIF4A and EIF3 as well as the RPS6 protein to initiate translation [40]. While we demonstrated that global translation is mandatory for degradation activity induced by invadosomes, the inhibition of global translation did not prevent invadosome formation (excepted for rosettes). Nevertheless, we also showed that ER-associated translation regulates all type of invadosomes formation suggesting that ER has a major role in invadosome formation and the associated degradation activity. We hypothesize that ribosome docking to ER, through Sec61, enhances protein synthesis of determinant elements for invadosome formation. A recent study demonstrated that an early increase of Sec61 enhanced the expression of pro-invasive proteins, followed by an expansion of the ER and the Golgi, leading to the delivery of these pro-invasive proteins to the cell membrane[41].

In addition to the translation proteins identified, proteins present in the ER have also been highlighted by our proteomic analysis such as RTN4 or LRRC59. Since ER is also involved in protein translation, this suggested the presence of a complex translation mechanism within all invadosomes. We showed that the ER is recruited at the rosette, so enrichment of the ER could be linked to the rosette functioning properly, notably for its degradation capacity. In addition, our data show that removal of the ER leads to a collapse of the rosette structure suggesting a link between ER and invadosome formation and degradation activity. Furthermore, we showed that the ER was necessary for initiating and maintaining the invadosome rosettes. Indeed, the spatiotemporal aspect of invadosome formation in the initiation, stabilization or collapse phases is a major question[42,43]. Here, we show that the ER plays a main role in these different stages.
In literature, Pedersen et *al.* also showed the involvement of ER in invadosome formation: protrudin mediated ER-endosome contact site promotes cell invasion through the translocation of MT1-MMP endosome to the plasma membrane leading to invadopodia outgrowth and degradation[31]. Moreover, one of our recent study showed that two ER proteins, calnexin and ERp57, can be trafficked to invadosomes and are essential for ECM degradation[32]. These results therefore suggest the presence of a complex allowing invadosomes to have their own translation machinery to facilitate cell invasion with local translation of specific mRNA[21,44]. Tks5 could therefore act as a molecular crossroads allowing translational proteins to cluster in the same place, leading to rapid localization and greater efficiency for the cell in the formation and function of invadosomes.

In order to better understand the link between the translation and the ER in all types of invadosomes, we first targeted the EIF4B protein, identified by mass spectrometry. Using siRNA strategy, we showed that EIF4B is required in degradation function. Recent studies already showed the involvement of EIF4B in invasion. Indeed, Cao and al. showed that the pathway PIM1/EIF4B/c-MET pathway was involved in tumor migration and invasion in lung adenocarcinoma[45]. In the same way, the GMAN/p-EIF4B pathway leads to cell proliferation and invasion in hepatocellular carcinoma (HCC)[46].
We also identified many proteins associated with EIF3 and EIF4 complexes such as EIF3C, EIF4A3, EIF4E or EIF3H in at least three out of four types of invadosomes. Similarly, these complexes are already known in the literature to participate in the process of cell invasion. The YTHDF1/EIF3C axis is involved in the invasion process in ovarian cancer[47], EIF3H participates to the invasion of hepatocellular carcinoma[48] and the EIF4A3/FLOT1 pathway promotes invasion and tumor proliferation in lung adenocarcinoma[49]. These results suggest the

involvement of these complexes in the degradation mechanism that could be common to all types of invadosomes.

Altogether, these results provide new knowledge specifically into invasive structures and on the invasion process more broadly. Indeed, we reported new molecular components common to all types of invadosomes through the identification of Tks5 interactome. This thus provides a better understanding of the mode of operation of invadosomes, in particular via the involvement of the ER-associated translation machinery which is involved into invadosome formation.

Material and methods

Antibodies and reagent

Anti-GFP (catalog number ab6673) antibody was purchased from Abcam. Anti-Tks5 (G-7, catalog number sc-376211), and anti-CD44 (DF1485, catalog number sc-7297) were purchased from Santa Cruz Biotechnology, Inc. Anti-MAP4 (AG1741, catalog number 11229-1-AP) was purchased from Proteintech. Anti-RPS6 (S369, catalog number AP22299a) was purchased from Abgent. Anti-DDK (OTI2F7, catalog number TA500288) was purchased from OriGene Technologies, Inc. Anti-EIF4B (catalog number 3592) was purchased from Cell Signaling Technology. Secondary antibodies for immunofluorescence IRDye® 680RD Conjugated Goat anti-mouse (926-68070, LI-COR Biotech.), IRDye® 680RD Conjugated Goat anti-rabbit, (926-68071, LI-COR Biotech.), IRDye® 800CW Conjugated Goat anti-mouse (926-32210, LI-COR Biotech.), IRDye® 800CW Conjugated Goat anti-rabbit (926-32211, LI-COR Biotech.). The Atto 647N conjugated Goat anti-mouse-IgG was purchased from Sigma-Aldrich (catalog number 50185). DAPI (catalog number H21486), phalloidin (catalog number FP-BZ-9630) were purchased from Interchim. Type I collagen from rat tail(catalog number 354236) was purchased from Corning. Sec61 translocon was inhibited by pharmacological approach using Eeyarestatin 1 (ES1, catalog number E1286 Sigma-Aldrich) at 5µM during 1 hour. Species-specific fluorescent far-red coupled secondary antibody for western blot IRDye 680CW goat (polyclonal) anti-rabbit IgG (H+L) (catalog number 926-68070) or IRDye 800CW goat (polyclonal) anti-mouse IgG (H+L) (catalog number 926-32210) were purchased from LI-COR Biotech. GM6001 MMP Inhibitor (catalog number CC10), Cycloheximide (CHX) (catalog number 01810) and Manganese(II) (catalog number M7899) were purchased from Sigma-Aldrich.

Cell culture

The A431 cell line was generously donated by Dr. Julie Dechanet-Merville (CNRS 5164, Bordeaux) and authenticated. NIH-3T3-Src cells were generously donated by Dr. Sara Courtneidge (Université of Portland, USA). A431 and NIH-3T3-Src cells were maintained in DMEM high glucose (Gibco) supplemented with 10% fetal bovine serum (FBS, 139 Sigma Aldrich) at 37°C in a 5% CO2 incubator. In this study, we used A431 and NIH-3T3-Src cells transduced with a lentiviral plasmid expressing Tks5 fused to GFP, and the cell line was named A431-Tks5-GFP and NIH3T3-Src-Tks5-GFP.

Lentiviral transduction

A431 and NIH-3T3-Src cells were seeded in a 6-well plate, then transduced after 24 h at a multiplicity of infection of 10 µg, either with a lentiviral plasmid containing Tks5 couple to GFP, or with the GFP alone plasmid encoding as a control . The transduced cells were selected using puromycin treatment at 1µg/mL. Co-transduction of lifeact-mRuby and KDEL-GFP NIH-3T3-Src cells has been performed as described above but double positive cells were selected and sorted using BD FACSAria Cell Sorter (BD Bioscience).

Transfection

EIF4B-DDK plasmid was purchased from OriGene Technologies, Inc. This plasmid was transfected (2,4 µg) using JetPrime (PolyPlus Transfection) following the manufacturer's instructions. siRNA oligonucleotides (20 nM) targeting eIF4B (Human: s4573 & s4574; Mouse: s93804 & s93805 ThermoFisher) were transfected using Lipofectamine RNAiMax (Invitrogen) according to the manufacturer's instructions.

Coating of coverslips with extracellular matrix (ECM)

Cells were seeded on gelatin coverslips with or without coating of collagen. Type I collagen (rat tail, catalog number 354236, Corning) was diluted in DPBS containing calcium and magnesium (Dulbecco's Buffered-Phosphate Saline, Gibco) at a final concentration of 0.5mg/ml and polymerized for 4 h at 37°C. Gelatin-coated coverslips were made using gelatin from Sigma-Aldrich (catalog number G1393). Coverslips were incubated with gelatin for 20 min before and then fixed with 0.5% glutaraldehyde (Electron Microscopy Science) for 40 min at room temperature. Coverslips were washed 3 times with PBS before cell seeding.

Immunofluorescence and imaging

Cells were fixed using 4% paraformaldehyde (PFA) (Electron Microscopy Sciences) for 10 min at room temperature and then rinsed 3 times with PBS. Cells were permeabilized using 0.2% Triton X-100 (catalog number T9284, Sigma-Aldrich) for 10 min at room temperature before being rinsed twice with PBS. Cells were then incubated with primary antibodies (1:100 diluted in PBS-4%BSA) for 40 min at room temperature, rinsed 3 times with PBS. The cells were then incubated with secondary antibodies (1:200 diluted in PBS-4%BSA) for 30 min at room temperature. Nuclei were stained with DAPI (1:1,000 dilution) and actin was stained with phalloidin (1:200 dilution). Coverslips were mounted on microscope slides using Fluoromount-G mounting media (catalog number 0100-01, SouthernBiotech) and were imaged using SP5

confocal microscope (Leica, Leica Microsystems GmbH, Wetzlar, Germany). Collagen is observed by internal reflection microscopy (IRM). Images were analyzed using ImageJ or Fiji softwares.

Live-cell imaging

Cells were seeded on glass bottom dishes then image acquisitions were performed every 2 min for 4 using LiveSR spinning-disk microscope (Leica, Leica Microsystems GmbH, Wetzlar, Germany) with environmental control at 37°C and CO_2 provider. Z-stacks were performed then deconvolution imaging were used for 3D reconstruction (Imaris software).

Correlative light and electron microscopy (CLEM)

For performing CLEM of invadosome rosettes, we did micro-pattern on ACLAR® films (Catalog number 77850-12, EMS) by the laser microdissection[50]. Solution of gelatin (0.5 mg/mL) was pre-coated on these patterned ACLAR® substrates in a 24-well plate. The lifeact-mRuby expressed NIH-3T3-Src cells were then seeded at 20,000 cells/mL on ACLAR® films and incubated overnight. The film was transferred to a 35mm glass bottom dish (Catalog number P35G-1.0-20-C, MatTek) for confocal imaging (Leica SP2) using a × 63 objective (NA:1.32, Leica Microsystems). Position of the region of interest (ROI) according to the landmarks visible in transmitted light. High-magnification images of the cells and rosettes of interest were acquired as well as low-magnification images. After imaged, cells were fixed in primary fixation buffer contained 2.5% PFA (Catalog number 15713, EMS) and 2.5% GA (Catalog number 16220, EMS) in 0.1M cacodylate buffer (Catalog 11652, EMS) for 1 h at room temperature. Post-fixation was performed in 1% osmium tetroxide (Catalog number 19150, EMS) in 0.1M cacodylate buffer for 1 h on ice. Cells were stained with 2% uranyl acetate, and then dehydrated in sequential gradient alcohol baths and infiltrated with Epon resin. We then inversed the film on the top of the plastic embedding capsule (Catalog number 69910-05, EMS) following overnight polymerization at 60 °C thus embedding the intact cell monolayer of adhesion cells. The following day, the capsules were filled with fresh Epon and polymerized again overnight at 60 °C. Accurate positioning of the ROI can be relocated by a stereomicroscope according to the micro-pattern. Finally, the precise trimmed resin block was done serial sectioning (thickness: 70 nm) and all the sections were collected on slot grids for TEM observation. Micrographs were obtained at transmitted electron microscope (CM12, FEI company) with a CCD camera (ORIUS, Gatan). For the image process, overlay the fluorescent

and the EM images in Fiji, and manually rescale or rotate the data until the cell boundaries align.

Western Blot

Cells were washed once with cold PBS on ice, and then were scraped with RIPA lysis buffer containing phosphatase and protease inhibitor cocltails (catalog number 04906845001, Merck) and lysed for 30 min on ice. Cell lysates were clarified by centrifugation at 13,000g for 15 min at 4°C. Protein concentrations were determined using BCA reagent (DC™ Protein Assay, BioRad), according to the manufacturer's protocol. Lysates were heat at 95°C for 10 min and then separated by SDS-PAGE electrophoresis on 10% acrylamide gels (FastCast™ Acrylamide kit, BioRad) at 110V for 60 min. Samples were transferred onto nitrocellulose membranes using a Transblot transfer system (BioRad) and membranes were blocked using 5%BSA with0.2%Tween (catalog number P7949, Sigma-Aldrich) in TBS buffer (catalog number ET220, Euromedex) for 1 h at room temperature before being incubated with primary antibodies (1:1,000 dilutiond in blocking buffer as described above) overnight at 4°C. The next day, membranes were washed 3 times with TBST and incubated with secondary antibodies (1:5,000 dilution with 5% BSA inTBST) for 30min at room temperature. Membranes were washed 3 times with TBST before exposure using a Chemidoc system (BioRad).

Immunoprecipitation

For immunoprecipitation experiments, 4.5 million cells were necessary and technical triplicate were performed. NIH-3T3-Src-Tks5-GFP and A431-Tks5-GFP cells were seeded on plastic or in dishes with a fibrillar collagen I matrix. Lysates were centrifuged for 15 min at 13,000g at 4°C and supernatants were immunoprecipitated with the GFP-Trap®_MA kit (Goldstandard) according to the supplier(s) recommendations. The immunoprecipitates were washed three times in lysis buffer, and then assayed using the Lowry method (DC™ Protein Assay kit, Biorad) using a spectrophotometer at 750nm.

Mass spectrometry

The steps of sample preparation and protein digestion by the trypsin were performed as previously described[51]. NanoLC-MS/MS analysis were performed using an Ultimate 3000 RSLC Nano-UPHLC system (Thermo Scientific, USA) coupled to a nanospray Q Exactive Hybrid Quadruplole-Orbitrap mass spectrometer (Thermo Scientific, USA). Each peptide extracts were loaded on a 300 µm ID x 5 mm PepMap C_{18} precolumn (Thermo Scientific, USA)

at a flow rate of 20 µL/min. After a 5 min desalting step, peptides were separated on a 75 µm ID x 25 cm C_{18} Acclaim PepMap® RSLC column (Thermo Scientific, USA) with a 4-40% linear gradient of solvent B (0.1% formic acid in 80% ACN) in 108 min. The separation flow rate was set at 300 nL/min. The mass spectrometer operated in positive ion mode at a 1.8 kV needle voltage. Data were acquired using Xcalibur 3.1 software in a data-dependent mode. MS scans (m/z 350-1600) were recorded at a resolution of R = 70000 (@ m/z 200) and an AGC target of 3 x 10^6 ions collected within 100 ms. Dynamic exclusion of selected precursors was set to 30 s and top 12 ions were selected from fragmentation in HCD mode. MS/MS scans with a target value of 1 x 10^5 ions were collected with a maximum fill time of 100 ms and a resolution of R = 17500. Additionally, only +2 and +3 charged ions were selected for fragmentation. Other settings were as follows: no sheath and no auxiliary gas flow, heated capillary temperature, 200°C; normalized HCD collision energy of 27% and an isolation width of 2 m/z. Protein identification and Label-Free Quantification (LFQ) were done in Proteome Discoverer 3.0. CHIMERYS node using prediction model inferys_2.1 fragmentation was used for protein identification in batch mode by searching against a Uniprot *Homo sapiens* database (82 439 entries, release March 2023) or a UniProt Mus musculus database (55 029 entries, release March 2023). Two missed enzyme cleavages were allowed for the trypsin. Peptide lengths of 7-30 amino acids, a maximum of 3 modifications, charges between 2-4 and 20 ppm for fragment mass tolerance were set. Oxidation (M) and carbamidomethyl (C) were respectively searched as dynamic and static modifications by the CHIMERYS software. Peptide validation was performed using Percolator algorithm[52] and only "high confidence" peptides were retained corresponding to a 1% false discovery rate at peptide level. Minora feature detector node (LFQ) was used along with the feature mapper and precursor ions quantifier. The normalization parameters were selected as follows: (1) Unique peptides, (2) Precursor abundance based on intensity, (3) No normalization was applied, (4) Protein abundance calculation: summed abundances, (5) Protein ratio calculation: pairwise ratio based and (6) Missing values are replaced with random values sampled from the lower 5% of detected values. Quantitative data were considered for master proteins, quantified by a minimum of 2 unique peptides, a fold changes ≥ 2 and a bilateral heteroscedastic t-test was applied (p-value < 0.05).

Inhibition of translation machinery present in invadosomes

A431-Tks5-GFP and NIH-3T3-Src-Tks5-GFP cells were seeded on coverslips coated with gelatin (dots/rosettes) or gelatin and type I collagen (linear invadosomes). The cells were treated with 35µM of translation inhibitor cycloheximide (CHX) (01810, Sigma-Aldrich) or DMSO

(control) (D8418, Sigma-Aldrich) 2 h after seeding. For cells seeded on collagen, cells were fixed 4h after seeding. For cells seeded on gelatin, cells were fixed 24 h after seeding by using 4% PFA. The immunofluorescence was performed as previously described. A total of 10 images were performed for each condition using a confocal microscope (SP5, Leica) and experiments were done in three biological replicates. The number of invadosomes were quantified using ImageJ and normalized to the number of nuclei. For Western Blot analysis, cells were seeded on plate and treated with 35µM of cycloheximide (CHX) or DMSO (control) 2h after seeding. Before extraction, cells were treated with Puromycin at a concentration of 10µg/mL. Western Blot was performed as previously described.

Image analysis of fluorescence intensities and area of gelatin degradation

Sterile coverslips were coated with Oregon Green™ 488 conjugated gelatin 488 (catalog number G13186, Thermofisher) for 20 min and fixed with 0.5% glutaraldehyde (catalog number 15960, EMS) for 40 min. Then, the same experiment as described before was performed. Coverslips were imaged under the epifluorescence microscope (Zeiss) using the x 63 oil immersion objective. A total of 15 images were acquired for each condition, and experiments were done in three biological replicates. The area of degradation was quantified using ImageJ and normalized to the number of nuclei in each image.

Statistical analysis

Data are reported as the mean ± SEM of at least three experiments. Statistical significance ($p < 0.05$ or less) was determined using analysis of variance (ANOVA) (one way, two way followed by a Bonferroni's correction), unpaired or paired student t-test as appropriate and performed with GraphPad Prism software. Significance levels are shown as p-values.

Data and material availability

The mass spectrometry proteomics data have been deposited to the ProteomeXchange Consortium via the PRIDE[53] partner repository with the dataset identifiers PXD046512 (NIH cells) and PXD046515 (A431 cells).

References

1. Ferrari, R. *et al.* MT1-MMP directs force-producing proteolytic contacts that drive tumor cell invasion. *Nat. Commun.* **10**, 4886 (2019).
2. Watanabe, A. *et al.* Critical Role of Transient Activity of MT1-MMP for ECM Degradation in Invadopodia. *PLoS Comput. Biol.* **9**, (2013).
3. Fekete, A. *et al.* EGF regulates tyrosine phosphorylation and membrane-translocation of the scaffold protein Tks5. *J. Mol. Signal.* **8**, 8 (2013).
4. Daubon, T., Spuul, P., Alonso, F., Fremaux, I. & Génot, E. VEGF-A stimulates podosome-mediated collagen-IV proteolysis in microvascular endothelial cells. *J. Cell Sci.* **129**, 2586–2598 (2016).
5. Varon, C. *et al.* Transforming Growth Factor β Induces Rosettes of Podosomes in Primary Aortic Endothelial Cells. *Mol. Cell. Biol.* **26**, 3582–3594 (2006).
6. Jerrell, R. J. & Parekh, A. Matrix Rigidity Differentially Regulates Invadopodia Activity Through ROCK1 and ROCK2. *Biomaterials* **84**, 119–129 (2016).
7. Parekh, A. *et al.* Sensing and Modulation of Invadopodia across a Wide Range of Rigidities. *Biophys. J.* **100**, 573–582 (2011).
8. Cannone, S. *et al.* Cancer Associated Fibroblast (CAF) Regulation of PDAC Parenchymal (CPC) and CSC Phenotypes Is Modulated by ECM Composition. *Cancers* **14**, 3737 (2022).
9. Juin, A. *et al.* Discoidin domain receptor 1 controls linear invadosome formation via a Cdc42–Tuba pathway. *J. Cell Biol.* **207**, 517–533 (2014).
10. Iizuka, S. *et al.* Crosstalk between invadopodia and the extracellular matrix. *Eur. J. Cell Biol.* **99**, 151122 (2020).
11. Di Martino, J. *et al.* The microenvironment controls invadosome plasticity. *J. Cell Sci.* **129**, 1759–1768 (2016).

12. Mueller, S. C. *et al.* A Novel Protease-docking Function of Integrin at Invadopodia*. *J. Biol. Chem.* **274**, 24947–24952 (1999).
13. Beaty, B. T. & Condeelis, J. Digging a little deeper: the stages of invadopodium formation and maturation. *Eur. J. Cell Biol.* **93**, 438–444 (2014).
14. Helgeson, L. A. & Nolen, B. J. Mechanism of synergistic activation of Arp2/3 complex by cortactin and N-WASP. *eLife* **2**, e00884 (2013).
15. Di Martino, J. *et al.* Cdc42 and Tks5. *Cell Adhes. Migr.* **8**, 280–292 (2014).
16. Seals, D. F. *et al.* The adaptor protein Tks5/Fish is required for podosome formation and function, and for the protease-driven invasion of cancer cells. *Cancer Cell* **7**, 155–165 (2005).
17. Lock, P., Abram, C. L., Gibson, T. & Courtneidge, S. A. A new method for isolating tyrosine kinase substrates used to identify fish, an SH3 and PX domain-containing protein, and Src substrate. *EMBO J.* **17**, 4346–4357 (1998).
18. Wang, W. *et al.* The Role of TKS5 in Chromosome Stability and Bladder Cancer Progression. *Int. J. Mol. Sci.* **23**, 14283 (2022).
19. Moodley, S., Hui Bai, X., Kapus, A., Yang, B. & Liu, M. XB130/Tks5 scaffold protein interaction regulates Src-mediated cell proliferation and survival. *Mol. Biol. Cell* **26**, 4492–4502 (2015).
20. Buschman, M. D. *et al.* The Novel Adaptor Protein Tks4 (SH3PXD2B) Is Required for Functional Podosome Formation. *Mol. Biol. Cell* **20**, 1302–1311 (2009).
21. Ezzoukhry, Z. *et al.* Combining laser capture microdissection and proteomics reveals an active translation machinery controlling invadosome formation. *Nat. Commun.* **9**, 2031 (2018).
22. Stylli, S. S. *et al.* Nck adaptor proteins link Tks5 to invadopodia actin regulation and ECM degradation. *J. Cell Sci.* **122**, 2727–2740 (2009).

23. Thuault, S. *et al.* A proximity-labeling proteomic approach to investigate invadopodia molecular landscape in breast cancer cells. *Sci. Rep.* **10**, 6787 (2020).

24. Mader, C. C. *et al.* An EGFR-Src-Arg-cortactin pathway mediates functional maturation of invadopodia and breast cancer cell invasion. *Cancer Res.* **71**, 1730–1741 (2011).

25. Wang, Y. *et al.* ERβ promoted invadopodia formation-mediated non-small cell lung cancer metastasis via the ICAM1/p-Src/p-Cortactin signaling pathway. *Int. J. Cancer* **153**, 1287–1299 (2023).

26. Inoue, H. *et al.* A MAP1B–cortactin–Tks5 axis regulates TNBC invasion and tumorigenesis. *J. Cell Biol.* **223**, e202303102 (2024).

27. Zhao, P. *et al.* The CD44s splice isoform is a central mediator for invadopodia activity. *J. Cell Sci.* **129**, 1355–1365 (2016).

28. Challa, S. *et al.* Ribosome ADP-Ribosylation Inhibits Translation and Maintains Proteostasis in Cancers. *Cell* **184**, 4531-4546.e26 (2021).

29. Shahbazian, D. *et al.* Control of Cell Survival and Proliferation by Mammalian Eukaryotic Initiation Factor 4B. *Mol. Cell. Biol.* **30**, 1478–1485 (2010).

30. Mallawaaratchy, D. M. *et al.* Membrane Proteome Analysis of Glioblastoma Cell Invasion. *J. Neuropathol. Exp. Neurol.* **74**, 425–441 (2015).

31. Pedersen, N. M. *et al.* Protrudin-mediated ER–endosome contact sites promote MT1-MMP exocytosis and cell invasion. *J. Cell Biol.* **219**, e202003063 (2020).

32. Ros, M. *et al.* ER-resident oxidoreductases are glycosylated and trafficked to the cell surface to promote matrix degradation by tumour cells. *Nat. Cell Biol.* **22**, 1371–1381 (2020).

33. Fuentes, L. A., Marin, Z., Tyson, J., Baddeley, D. & Bewersdorf, J. The nanoscale organization of reticulon 4 shapes local endoplasmic reticulum structure in situ. *J. Cell Biol.* **222**, e202301112 (2023).

34. Hwang, Y. S., Park, K.-K., Cha, I. H., Kim, J. & Chung, W.-Y. Role of insulin-like growth factor-II mRNA-binding protein-3 in invadopodia formation and the growth of oral squamous cell carcinoma in athymic nude mice. *Head Neck* **34**, 1329–1339 (2012).
35. Hwang, Y. S., Xianglan, Z., Park, K.-K. & Chung, W.-Y. Functional invadopodia formation through stabilization of the PDPN transcript by IMP-3 and cancer-stromal crosstalk for PDPN expression. *Carcinogenesis* **33**, 2135–2146 (2012).
36. Kim, H.-Y., Ha Thi, H. T. & Hong, S. IMP2 and IMP3 cooperate to promote the metastasis of triple-negative breast cancer through destabilization of progesterone receptor. *Cancer Lett.* **415**, 30–39 (2018).
37. Tu, C. *et al.* Lysosomal cathepsin B participates in the podosome-mediated extracellular matrix degradation and invasion via secreted lysosomes in v-Src fibroblasts. *Cancer Res.* **68**, 9147–9156 (2008).
38. Li, D. *et al.* The lncRNA MIR99AHG directs alternative splicing of SMARCA1 by PTBP1 to enable invadopodia formation in colorectal cancer cells. *Sci. Signal.* **16**, eadh4210 (2023).
39. Chabadel, A. *et al.* CD44 and β3 Integrin Organize Two Functionally Distinct Actin-based Domains in Osteoclasts. *Mol. Biol. Cell* **18**, 4899–4910 (2007).
40. Magnuson, B., Ekim, B. & Fingar, D. C. Regulation and function of ribosomal protein S6 kinase (S6K) within mTOR signalling networks. *Biochem. J.* **441**, 1–21 (2011).
41. Costa, D. S. *et al.* The Caenorhabditis elegans anchor cell transcriptome: ribosome biogenesis drives cell invasion through basement membrane. *Development* **150**, dev201570 (2023).
42. Kreider-Letterman, G. *et al.* ARHGAP17 regulates the spatiotemporal activity of Cdc42 at invadopodia. *J. Cell Biol.* **222**, e202207020 (2022).

43. Badowski, C. *et al.* Paxillin Phosphorylation Controls Invadopodia/Podosomes Spatiotemporal Organization. *Mol. Biol. Cell* **19**, 633–645 (2008).

44. Zeng, H. *et al.* Spatially resolved single-cell translatomics at molecular resolution. *Science* **380**, eadd3067 (2023).

45. Cao, L. *et al.* PIM1 kinase promotes cell proliferation, metastasis and tumor growth of lung adenocarcinoma by potentiating the c-MET signaling pathway. *Cancer Lett.* **444**, 116–126 (2019).

46. Xu, J. *et al.* Long noncoding RNA GMAN promotes hepatocellular carcinoma progression by interacting with eIF4B. *Cancer Lett.* **473**, 1–12 (2020).

47. Liu, T. *et al.* The m6A reader YTHDF1 promotes ovarian cancer progression via augmenting EIF3C translation. *Nucleic Acids Res.* **48**, 3816–3831 (2020).

48. Tang, J. *et al.* The deubiquitinase EIF3H promotes hepatocellular carcinoma progression by stabilizing OGT and inhibiting ferroptosis. *Cell Commun. Signal. CCS* **21**, 198 (2023).

49. Yu, W. *et al.* EIF4A3 Acts on the PI3K–AKT–ERK1/2–P70S6K Pathway through FLOT1 to Influence the Development of Lung Adenocarcinoma. *Mol. Cancer Res.* **21**, 713–725 (2023).

50. Spiegelhalter, C., Laporte, J. F. & Schwab, Y. Correlative Light and Electron Microscopy: From Live Cell Dynamic to 3D Ultrastructure. in *Electron Microscopy* (ed. Kuo, J.) vol. 1117 485–501 (Humana Press, Totowa, NJ, 2014).

51. Henriet, E. *et al.* Argininosuccinate synthase 1 (ASS1): A marker of unclassified hepatocellular adenoma and high bleeding risk. *Hepatology* **66**, 2016 (2017).

52. Käll, L., Canterbury, J. D., Weston, J., Noble, W. S. & MacCoss, M. J. Semi-supervised learning for peptide identification from shotgun proteomics datasets. *Nat. Methods* **4**, 923–925 (2007).

53. Deutsch, E. W. *et al.* The ProteomeXchange consortium at 10 years: 2023 update. *Nucleic Acids Res.* **51**, D1539–D1548 (2022).

Acknowledgments:

The microscopy was done in the Bordeaux Imaging Center a service unit of the CNRS-INSERM and Bordeaux University, member of the national infrastructure France BioImaging supported by the French National Research Agency (ANR-10-INBS-04). The help of Magali Mondin is acknowledged. We are also grateful to platform of the unit TBMCore (US 005), Oncoprot and FACSility (US 005). We also thank Kuang-Jing Huang from U1109 for his help.

Author contributions:

L.N and B.B designed and performed experiments. S.D.T, J.W.D and A.A.R performed and interpreted mass spectrometry analysis. L.M and J.G contributed to CLEM analysis. L.N, B.B, V.M, E.H and FS wrote the manuscript, F.S designed and led the study.

Data Availability:

All data supporting the findings of this study are available from the corresponding author upon reasonable request. The mass spectrometry data are available via ProteomeXchange with the identifier PXD046512 (NIH cells) and PXD046515 (A431 cells). Source data are provided with this paper.

Funding:

Léa Normand was supported by a PhD scholarship from the SIRIC BRIO and the Région. Benjamin Bonnard was supported by the Inca. This work was supported by Fondation Ruban rose, Inca (PLBIO-2020-122) and Ligue contre le cancer (équipe labellisée 2023-DN/IP/IQ - 17691).

Figure legends

Figure 1: Invadosome plasticity.
a) Confocal microscopy images of invadosome formation in NIH3T3-Src cells. The cells were seeded on gelatin or type I collagen to form rosettes and linear invadosomes respectively. Tks5 is stained in green, actin in red, nuclei in blue and collagen fibers were imaged by internal reflection microscopy (IRM). Scale bar: 40µm, zoom: 5µm. **b)** Confocal microscopy images of invadosome formation in A431 cells. The cells were seeded on gelatin or type I collagen to formed dots and linear invadosomes respectively. Tks5 is stained in green, actin in red, nuclei in blue and collagen was imaged by internal reflection microscopy (IRM). The arrows show the collagen fibers. Scale bar: 40µm, zoom: 5µm.

Figure 2: Proteomic analysis of Tks5 interactome in invadosomes.
a) Confocal microscopy images of NIH3T3-Src-Tks5-GFP and A431-Tks5-GFP cells. The cells were seeded on gelatin and type I collagen to form invadosomes and stained for Tks5 and GFP. Scale bar: 5µm. **b)** Proteins interacting with Tks5-GFP by co-immunoprecipitation in NIH3T3-Src-Tks5-GFP and A431-Tks5-GFP cells on gelatin and type I collagen. 88 common proteins were identified in every conditions. **c)** List of the 88 commons proteins identified in every conditions. **d)** Bubble plot of the proteins related pathway. **e)** Confocal microscopy images of NIH-3T3-Src and A431-Tks5-GFP cells. The cells were seeded on gelatin or type I collagen and stained for Tks5 in green, actin in red, nuclei in blue and CD44 in grey. Scale bar: 20µm, zoom: 5µm.

Figure 3: The translation machinery is present in all types of invadosomes.
a) Confocal microscopy images of NIH3T3-Src-Tks5-GFP cells. The cells were seeded on gelatin or type I collagen and stained for Tks5 in green, actin in red, nuclei in blue and RPS6 in grey. Scale bar: 40µm, zoom: 10µm. **b)** Confocal microscopy images of A431-Tks5-GFP cells. The cells were seeded on gelatin or type I collagen and stained for Tks5 in green, actin in red, nuclei in blue and RPS6 in grey. Scale bar: 40µm, zoom: 10µm. **c)** Confocal microscopy images of NIH3T3-Src-Tks5-GFP cells. The cells were seeded on gelatin or type I collagen and stained for Tks5 in green, actin in red, nuclei in blue and Eif4b in grey. Scale bar: 40µm, zoom: 10µm. **d)** Confocal microscopy image of A431-Tks5-GFP cells. The cells were seeded on gelatin or type I collagen and stained for Tks5 in green, actin in red, nuclei in blue and Eif4b in grey. Scale bar: 40µm, zoom: 10µm.

Figure 4: Involvement of the translation machinery in invadosome activity.
a) Left: Quantification of the numbers of invadosomes per cell treated (CHX) or not (DMSO) with cycloheximide in NIH3T3-Src-Tks5-GFP cells seeded on gelatin. Values represent the mean +/- SEM of n=3 independent experiments (10 images per condition and per replicate) and were analyzed using student t-test. **b)** Representative images of the quantification of invadosome formation in NIH3T3-Src-Tks5-GFP cells seeded on gelatin. Tks5 is stained in green and nuclei in blue. Scale bar: 40µm, zoom: 10µm. **c)** Left: Quantification of the ECM degradation properties of A431 and NIH3T3-Src-Tks5-GFP cells on gelatin treated (CHX) or not (DMSO) with cycloheximide. Values represent the mean +/- SEM of n=3 independent experiments (15 images per condition and per replicate) and were analyzed using student t-test. Right: Representative images of the quantification of ECM degradation of A431 and NIH3T3-Src-Tks5-GFP cells on gelatin. Gelatin is stained in green and nuclei in blue. Scale bar: 40µm, zoom: 10µm. **d)** Left: Quantification of the ECM degradation properties of A431 and NIH3T3-Src-Tks5-GFP cells on collagen treated (CHX) or not (DMSO) with cycloheximide. Values represent the mean +/- SEM of n=3 independent experiments (15 images per condition and per

replicate) and were analyzed using student t-test. Right: Representative images of the quantification of ECM degradation of A431 and NIH3T3-Src-Tks5-GFP cells on collagen. Gelatin is stained in green and nuclei in blue. Scale bar: 40µm, zoom: 10µm. **e)** Left: Quantification of the ECM degradation properties of A431 and NIH3T3-Src-Tks5-GFP cells on gelatin treated (siEIF4B#1 and #2) or not (siCtrl) with siEIF4B. Values represent the mean +/- SEM of n=3 independent experiments (15 images per condition and per replicate) and were analyzed using student t-test. Right: Representative images of the quantification of ECM degradation of A431 and NIH3T3-Src-Tks5-GFP cells on gelatin. Gelatin is stained in green and nuclei in blue. Scale bar: 40µm, zoom: 10µm. **f)** Left: Quantification of the ECM degradation properties of A431 and NIH3T3-Src-Tks5-GFP cells on collagen treated (siEIF4B#1 and #2) or not (siCtrl) with siEIF4B. Values represent the mean +/- SEM of n=3 independent experiments (15 images per condition and per replicate) and were analyzed using student t-test. Right: Representative images of the quantification of ECM degradation of A431 and NIH3T3-Src-Tks5-GFP cells on collagen. Gelatin is stained in green and nuclei in blue. Scale bar: 40µm, zoom: 10µm.

Figure 5: Recruitment of ER into invadosome rosettes.
a) Bubble plot of proteins related pathway identified by mass spectrometry thanks to Tks5 and present in data already published by Ezzoukhry and *al.* in rosettes. **b)** Representative images from time-lapse video microscopy of lifeact-mRuby (red)-expressing NIH-3T3-Src cells transfected with KDEL-GFP (white). The lifeact-mRuby and KDEL-GFP were measured along the yellow axis. Scale bar: 20µm. **c)** Projection of a z-stacks and Imaris surface 3D renderings are shown, visualizing that KDEL-GFP (green) localizes inside invadosome during maturation. Scale bar: 20µm. **d)** CLEM images of invadosomes of NIH-3T3-Src cells on gelatin matrix. Actin is stained in red. Scale bar: 10µm and 1µm. **e)** Representative images from time-lapse video microscopy of lifeact-mRuby (red)-expressing NIH-3T3-Src cells transfected with KDEL-GFP (white). Intensity level of lifeact-mRuby and KDEL-GFP were measured in initiation step in rosette. Scale bar: 5µm. **f)** Representative images from time-lapse video microscopy of lifeact-mRuby (red)-expressing NIH-3T3-Src cells transfected with KDEL-GFP (white). Intensity level of lifeact-mRuby and KDEL-GFP were measured in maintained and collapsed in rosettes. Scale bar: 5µm. **g)** Projection of a z-stacks and Imaris surface 3D renderings are shown, visualizing that KDEL-GFP (green) escape from invadosome during his collapse. Scale bar: 20µm.

Figure 6: Involvement of ER-associated machinery translation in invadosome formation.
a) Lifeact-mRuby and KDEL-GFP signals were recorded in NIH-3T3-Src cells treated with cycloheximide (CHX; 35µM) at T60 min. Scale bar: 5 µm. **b)** Upper part: Quantification of invadosome formation in A431 and NIH-3T3-Src cells seeded on gelatin or type 1 collagen treated or not (DMSO) with Sec61 translocon inhibitor (ES1) during one hour. Lower part: Representative images of the quantification of invadosomes formation in A431 and NIH3T3-Src-Tks5-GFP cells seeded on gelatin or type 1 collagen treated or not (DMSO) with ES1. The arrows show the invadosomes. Tks5 is stained in green and nuclei in blue. Scale bar: 40µm, zoom: 10µm.

Supp Figure 1: Specific molecular signature of each invadosomes organizations.
a) Western Blot analysis of the co-immunoprecipitation performed with anti-GFP antibodies in NIH3T3-Src-Tks5-GFP cells. The input, the Δ and the co-IP (IP-Tks5-GFP) fractions are shown. **b)** Bubble plot of the proteins related pathway in rosettes. **c)** Classification table of the specific proteins identified in rosette. Proteins are grouped into five main categories corresponding to translation proteins, mitochondrial proteins, ER proteins, proteins of the Golgi

apparatus and microtubules proteins. **d)** Bubble plot of the proteins related pathway in dots. **e)** Classification table of the specific proteins identified in dots. Proteins are grouped into five main categories corresponding to translation proteins, mitochondrial proteins, ER proteins, proteins of the Golgi apparatus and microtubules proteins. **f)** Bubble plot of the proteins related pathway in linear invadosomes and classification table of the adhesion proteins specific to linear invadosomes organizations. **g)** Classification table of the specific proteins identified in linear invadosomes. Proteins are grouped into five main categories corresponding to translation proteins, mitochondrial proteins, ER proteins, proteins of the Golgi apparatus and microtubules proteins.

Supp Figure 2: Characterization and validation of proteins identified by mass spectrometry as partner of Tks5.
a) Table of proteins identified by mass spectrometry in at least one type of invadosomes and already identified in the literature as partner of Tks5 in 293T cells (Stylli and *al.*) and MDA-MB-231 cells (Thuault and *al.*). **b)** Confocal microscopy images of A431-Tks5-GFP cells. The cells were seeded on gelatin or type I collagen and stained for Tks5 in green, actin in red, nuclei in blue and MAP4 in grey. Scale bar: 40µm, zoom: 5µm. **c)** Classification table of the 88 common proteins identified. Proteins are grouped into three main categories corresponding to translation, adhesion and actin cytoskeleton.

Supp Figure 3: Translation is not involved on invadosome formation.
a) Table of translation proteins already identified in invadosomes in the literature. **b)** Quantification of the effect of cycloheximide treatment on A431 and NIH-3T3-Src cells by using puromycin quantification. Values represent the mean +/- SEM of n=3 independent experiments and were analyzed using student t-test. **c)** Relative western blot analysis of puromycin expression for cells treated (CHX) or not (DMSO) with cycloheximide in A431 and NIH-3T3-Src cells seeded on gelatin or collagen. **d)** Quantification of the numbers of invadosomes per cell on gelatin and collagen treated (CHX) or not (DMSO) with cycloheximide in A431-Tks5-GFP and NIH3T3-Src-Tks5-GFP cells. Values represent the mean +/- SEM of n=3 independent experiments (10 images per condition and per replicate) and were analyzed using student t-test. **e)** Representative images of invadosome formation in A431-Tks5-GFP1 and NIH3T3-Src-Tks5-GFP cells seeded on gelatin or collagen. Tks5 is stained in green and nuclei in blue. Scale bar: 40µm, zoom: 10µm. **f)** Western Blot analysis of endogenous EIF4B expression in A431 and NIH-3T3-Src cells transfected using control or EIF4B-targeting siRNA and associated quantification. Stain free was used as the loading control. Values represent the mean of n=3 independent experiments.

Video 1:
Time-lapse video microscopy of lifeact-mRuby (red)-expressing NIH-3T3-Src cells transfected with KDEL-GFP (white).

Video 2:
Time-lapse video microscopy of lifeact-mRuby (red)-expressing NIH-3T3-Src cells transfected with KDEL-GFP (white).

Video 3:
Time-lapse video microscopy of lifeact-mRuby (red)-expressing NIH-3T3-Src cells transfected with KDEL-GFP (white).

Video 4:

Time-lapse of Lifeact-mRuby and KDEL-GFP signals recorded in NIH-3T3-Src cells treated with cycloheximide (CHX; 35µM).

Figure 1 : Invadosomes plasticity.

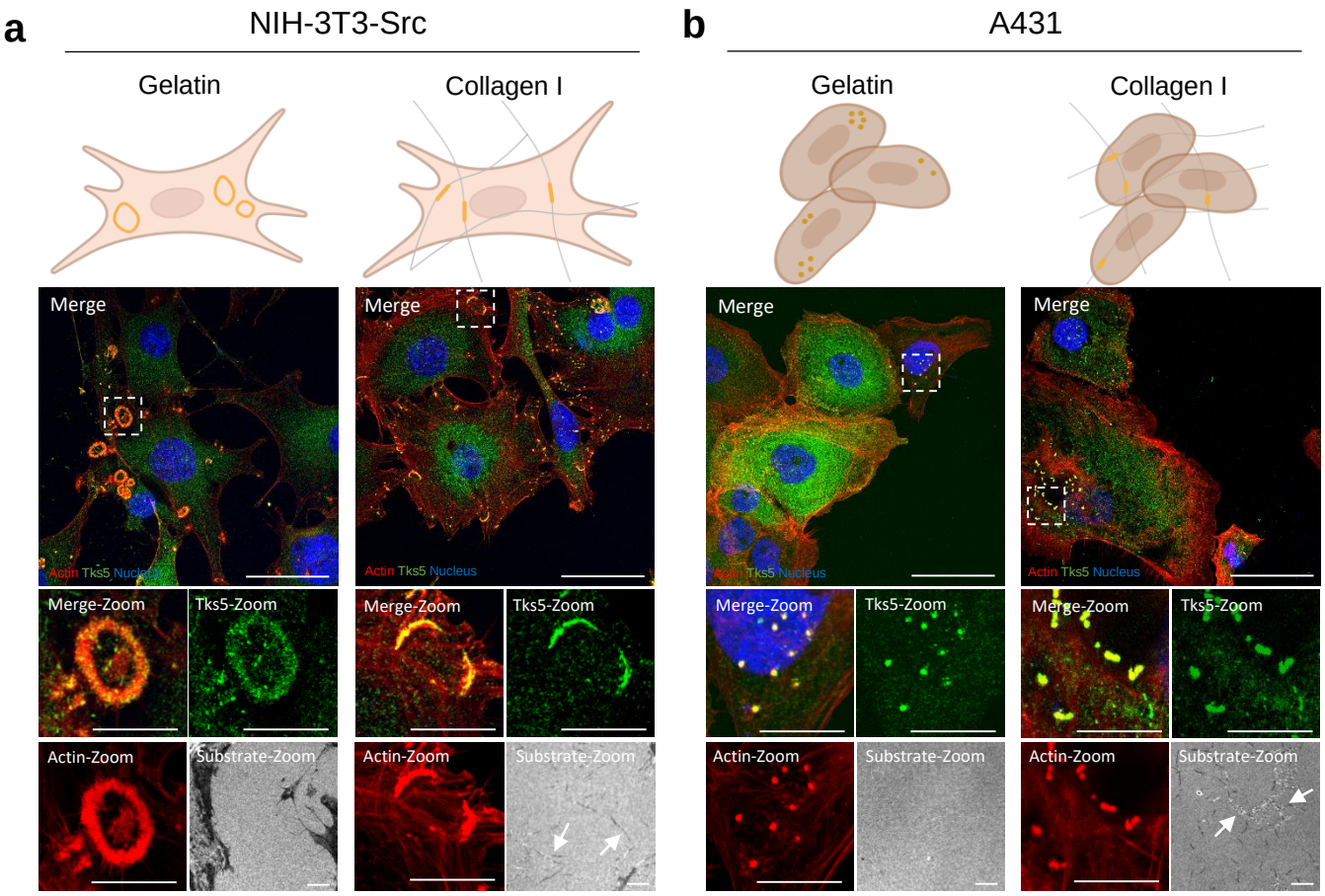

Figure 2 : Proteomic analysis of Tks5 interactome in invadosomes.

a

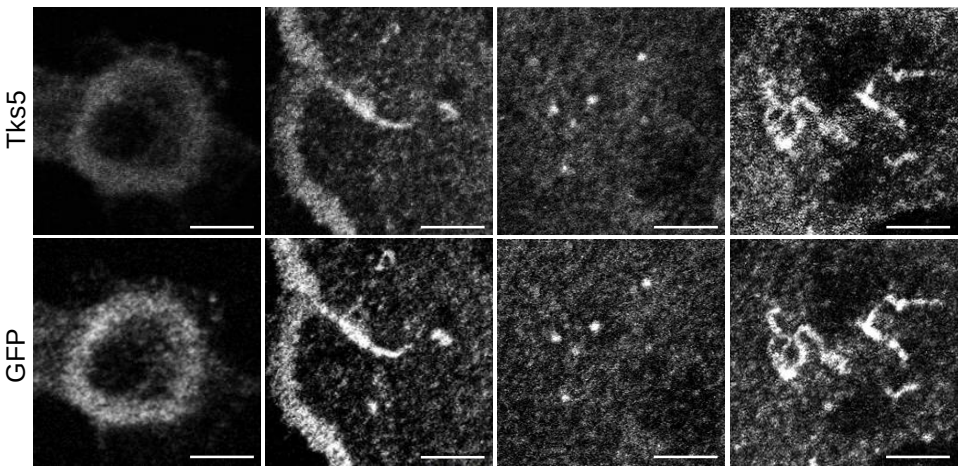

b

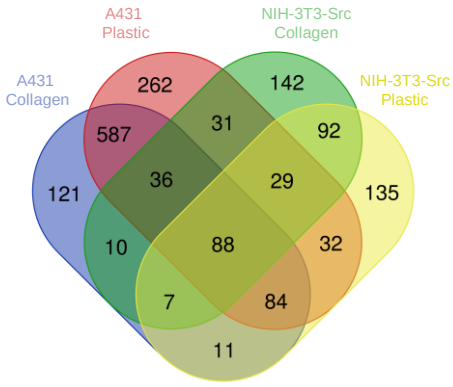

c

List of the 88 common proteins present in every conditions

Not validated in invadosomes
BASP1, BZW2, C1QBP, CLTB, DLD, EIF3A, EMD, GUSB, HNRNPAB, HNRNPU, LAMP2, LARP4, LRRC59, NUFIP2, PPM1G, PRKAG1, PRR2C2, PRRC2A, PSMD7, PUF60, PVR, RPL0, RPL3, RPL4, RPL5, RPL6, RPL7, RPL8, RPL7A, RPL13, RPL14, RPL15, RPL18A, RPL19, RPL29, RPL32, RPL36A, RPS6, RPS6KA4, RPS8, RTN4, RTRAF, SART1, SPATS2, SRSF1, STAU1, TCOF1, YBX1, YWHAB, YWHAE, YWHAG, YWHAH, YWHAQ, YWHAZ
Validated in at least one of the invadosomes organization
ADAM15, ADAM19, ASPH, BAG3, CALD1, CD44, CTTN, EIF4B, FNBP1L, FXR1, G3BP1, HNRNPA1, IGF2BP2, ITGA5, LAMP1, MAP4, MMP14, MYH9, NONO, NPM1, PABPC1, PPP1CA, PRKAA1, PTBP1, RPL10A, RPL34, RPS4X, RRBP1, SH3PXD2A, SSB, STX7, SYNCRIP, THBD, YBX3

d

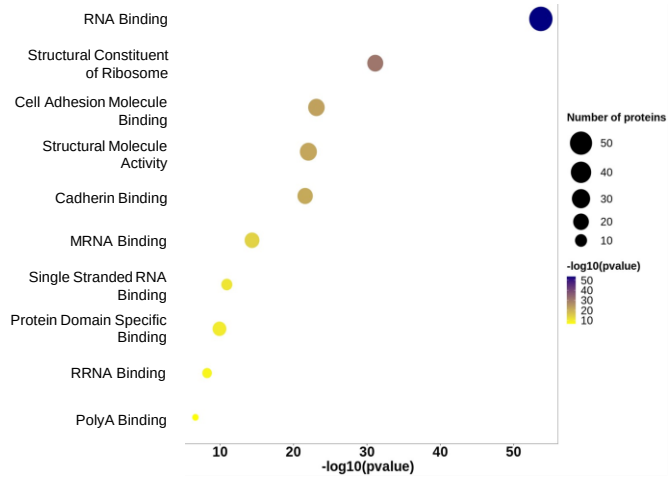

e

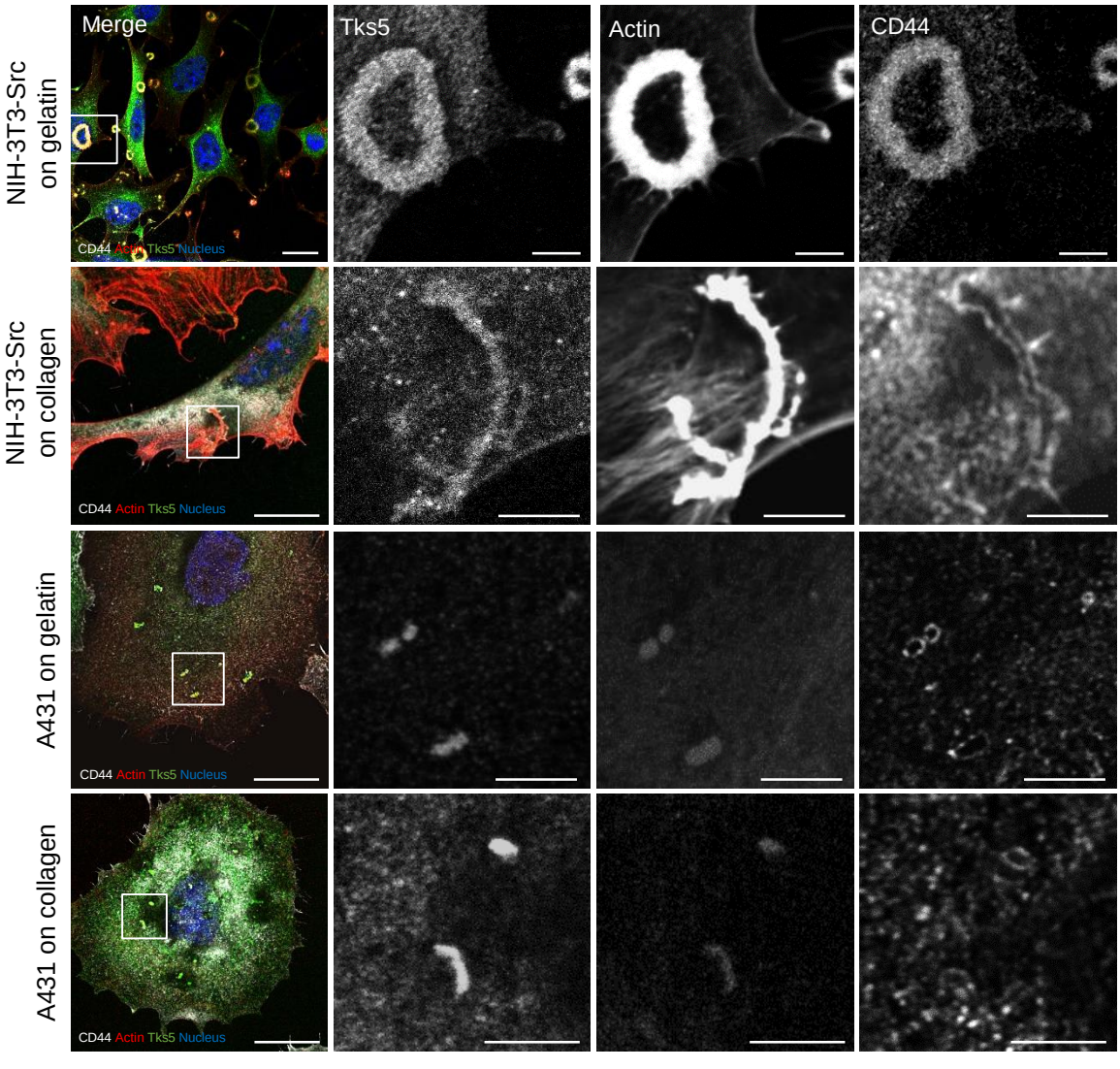

Figure 3 : The translation machinery is present in all types of invadosomes.

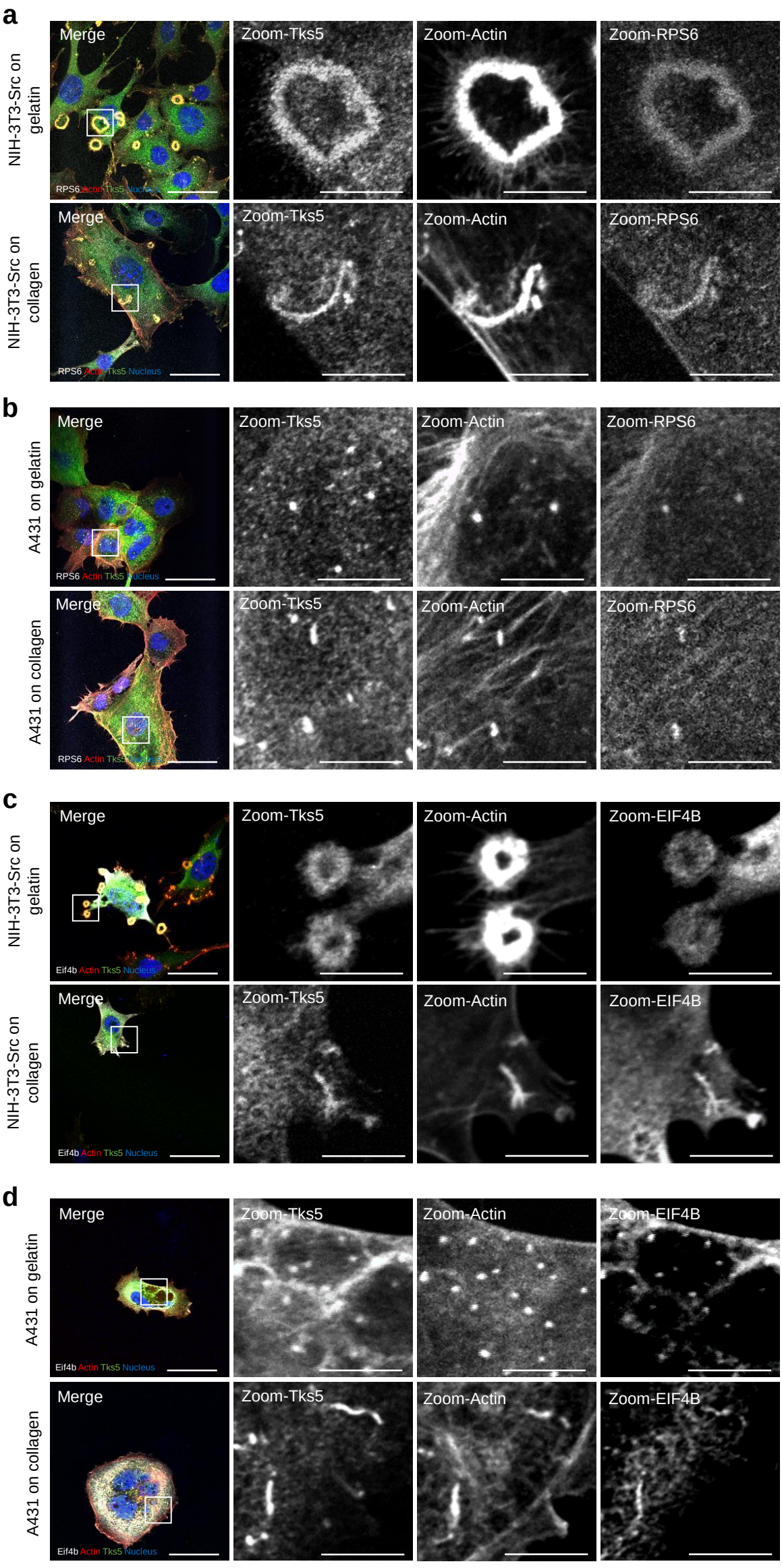

Figure 4 : Involvement of translation in invadosomes function.

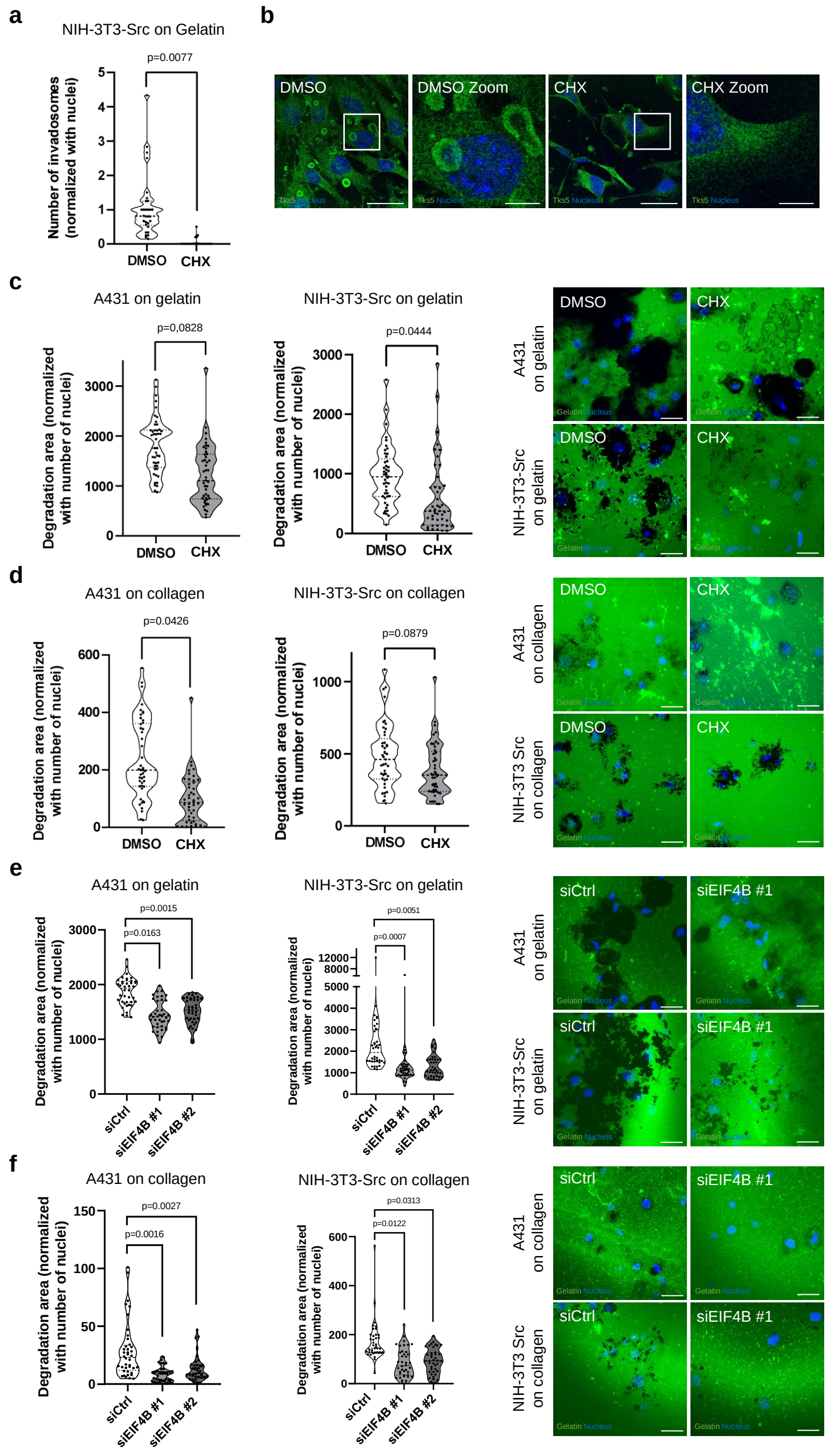

Figure 5 : Recruitment of ER into invadosomes rosettes.

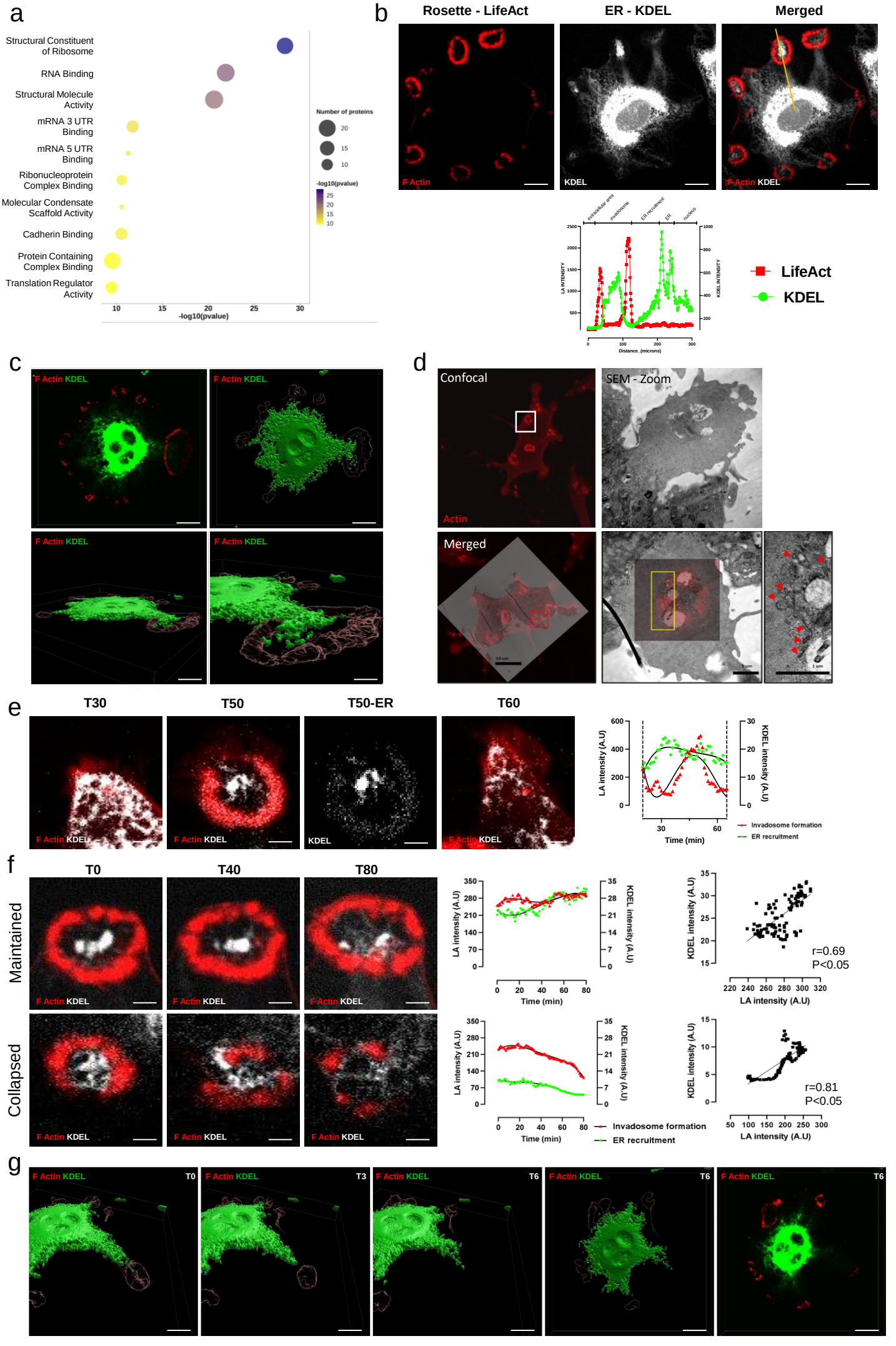

Figure 6 : Involvement of ER-associated machinery translation in invadosomes formation and function**.**

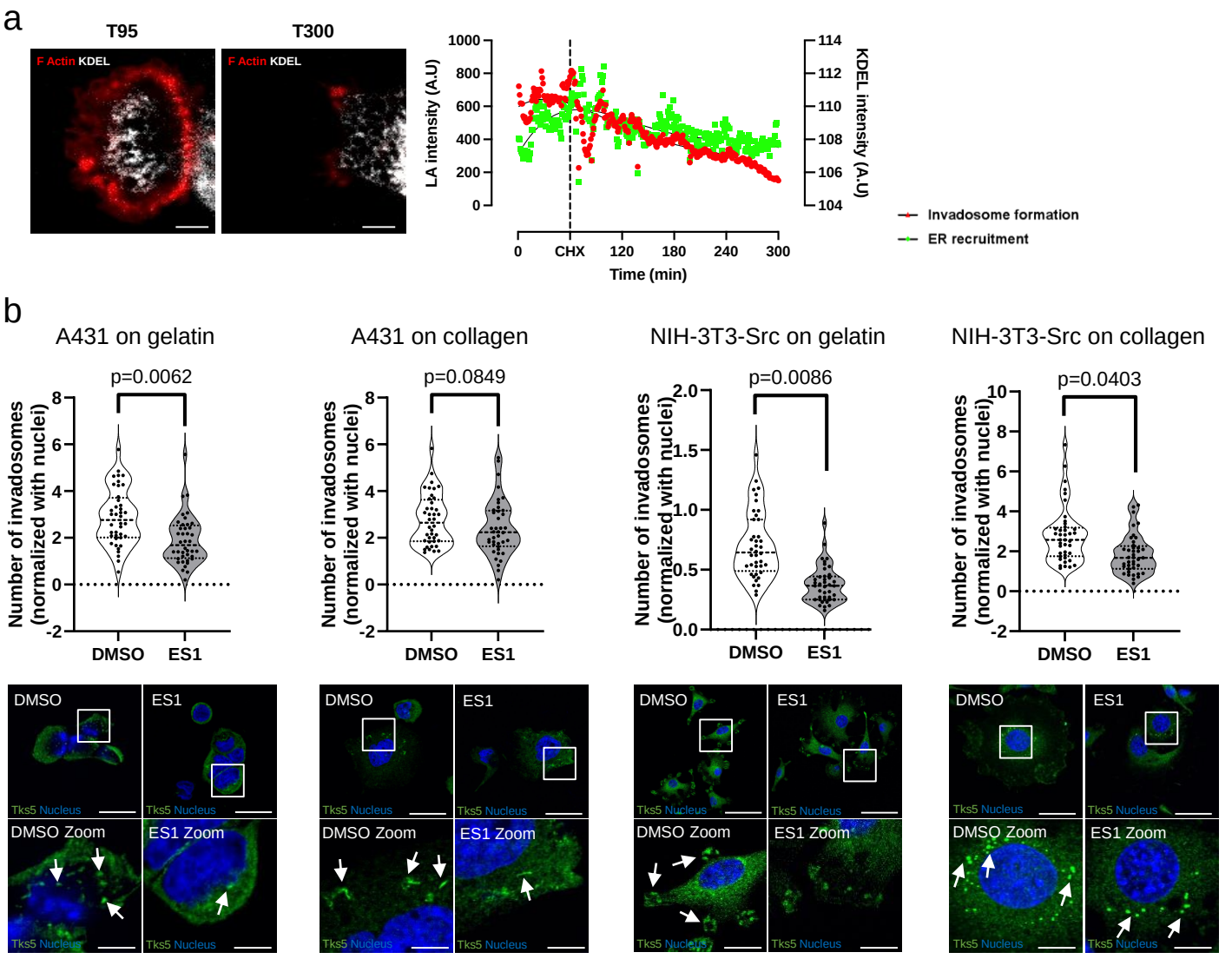

Supp Figure 1: Specific molecular signature of each invadosomes organizations.

a

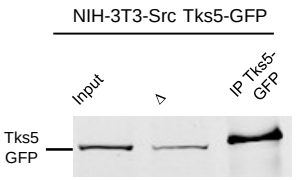

b

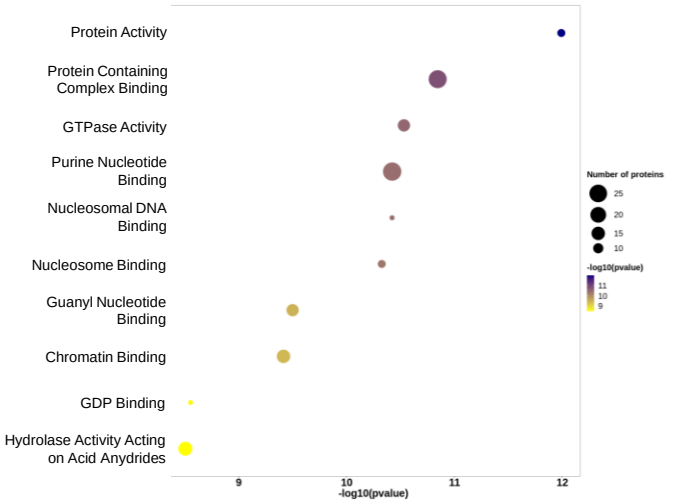

c

List of proteins present in rosettes

Translation proteins	EIF1A, EIF3S3X, EIF5A, MRPL12, NGDN
Mitochondrial proteins	AFG3L1, ATAD1, ATP5PB, MRPL12, NDUFV1, NFU1, PGAM5, RDH13, SLC25A4, SLC25A10, SLC29A1, SLC44A2
Endoplasmic reticulum proteins	CISD2, CNPY2, RAB1A, RAB1B, SEC22B, TMED9, TMX1, UBXN4
Proteins of the golgi apparatus	RAB1A, RAB1B, RAB6A, SEC22B, TMED9, TMED10
Microtubule proteins	STMN1

d

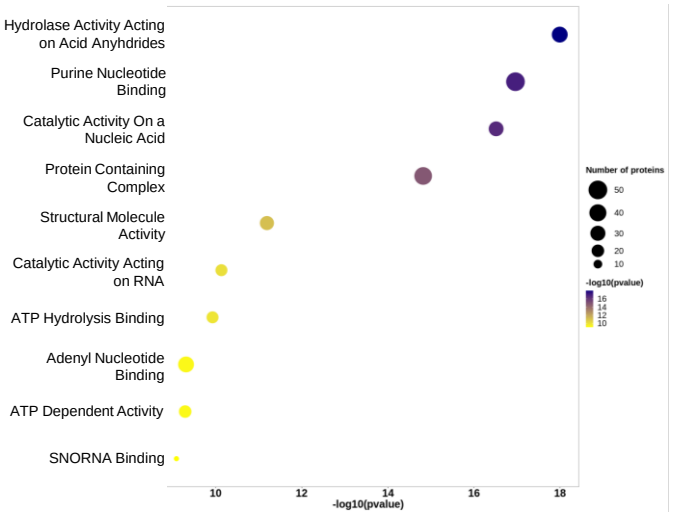

e

List of proteins present in dots

Translation proteins	BOP1, BRIX1, DDX27, EEFSEC, EIF3CL, EIF3I, EIF6, GNL2, IMP4, LARP4B, MRM3, MRPL2, MRPL15, MRPL37, MRPL47, MRPS12, MRPS15, MRPS23, MRPS34, NOP56, NSUN4, POLDIP3, RPS15, YTHDF1
Mitochondrial proteins	CHCHD3, CYC1, DIABLO, DRG1, GTF3C4, HK2, HTRA2, IMMT, MCAT, MRM3, MRPL2, MRPL15, MRPL37, MRPL47, MRPS12, MRPS15, MRPS23, MRPS34, NDUFA10, NDUFS2, NIPSNAP1, NSUN4, PRORP, PTPMT1, RAB38, RHOT1, SFXN3, SLC25A3B16, TEFM, VDAC1, VDAC2
Endoplasmic reticulum proteins	DHCR7, DNAJB11, DNAJC10, DPM1, EMC3, ERLIN2, HTRA2, PIGT, PRKAR2A, PUM3, RCN2, SEC61B, SEC62, SET, SLC35B2, SRP72, STT3A, SURF4, TAP2, TECR, TMCC1, TMEM214, TMX3, TOR1AIP2, UFL1
Proteins of the golgi apparatus	MGAT1, MYO18A, NSF, PRKAR2A, RAB34, SLC35B2, SURF4, TMEM214
Microtubule proteins	MARK3, TBCA, TMEM214, TTLL3, TUBB, TUBB4B

f

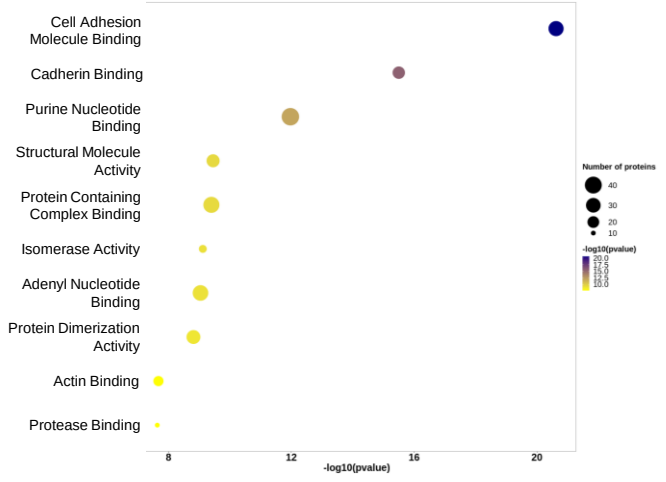

Adhesion proteins	CCN1, CD34, CD151, DAG1, ECM1, FN1, ITGB1, TSPAN6

g

List of proteins present in linear invadosomes

Translation proteins	DHX37, EEF1D, EIF2B4, EIF3J2, EIF3L, EIF5, EIF5B, ERAL1, MRPL44, PTCD1, PUM1, PYM1, RPS21, RWDD1
Mitochondrial proteins	ABCB7, ACADL, AFG3L2, AK4, AK4P3, ATP5MF, CLPX, DHODH, ECHS1, ERAL1, ETFA, ETFB, ETHE1, GFM1, GLUD1, HADH, HMGCL, HSPD1, IDH2, MFN1, MIX23, MRPL44, NDUFA4, PTCD1, PYCR1, TOMM70, YARS2
Endoplasmic reticulum proteins	ABHD12, ATL2, ATXN2, COPB1, CRELD2, ERAP1, ERLEC1, FKBP9, GOLT1B, HM13, LCLAT1, PIGK, PIGS, PLP2, SACM1L, SEC23IP, SSR1, UFD1
Proteins of the golgi apparatus	ARFGAP1, ARFIP1, COPB1, CRELD2, FAM20B, GOLGA5, GOLIM4, NSFL1C, STX6, TGOLN2, TMEM87A, USO1, VTI1A, YIPF3
Microtubule proteins	CEP170, DYNC1H1, MAP1B, MAP6, TACC2

Supp Figure 2 : Characterization and validation of proteins identified by mass spectrometry as partner of Tks5.

a

Proteins	A431 Gelatin	A431 Collagen	NIH-3T3-Src Gelatin	NIH-3T3-Src Collagen
ACTB	X	X		
CRKL	X			
CTTN	X	X	X	X
DBN1			X	X
DDX3X	X	X		
EEF2	X	X		
G3BP1	X	X	X	X
GRB2	X		X	
HNRNPK	X	X		
HSP90B1		X		
MARS1	X	X		
MTHFD1	X	X		
NDRG1	X	X		
NCL	X	X		
PRKAA1	X	X	X	X
PRKAG1	X	X	X	X
RUVBL1	X			
RUVBL2	X			

Stylli and *al.*, 2009

Proteins	A431 Gelatin	A431 Collagen	NIH-3T3-Src Gelatin	NIH-3T3-Src Collagen
ADAM15	X	X	X	X
ARAG	X	X		
CD2AP				X
CTTN	X	X	X	X
DBNL			X	X
EIF2S3	X	X		
EIF4A3	X	X	X	
FGD1	X	X	X	
FNBP1	X	X	X	X
HSPA1B	X	X		
IGF2BP2	X	X	X	X
MAP4	X	X	X	X
NAP1L1	X	X		
NUDT5	X			
PDLIM1				X
PRDX4	X			
RPIA				X
RTN4	X	X	X	X
SH3PXD2A	X	X	X	X
TJP1	X	X		
USP15	X	X		
WASL	X	X		

Thuault and *al.*, 2020

b

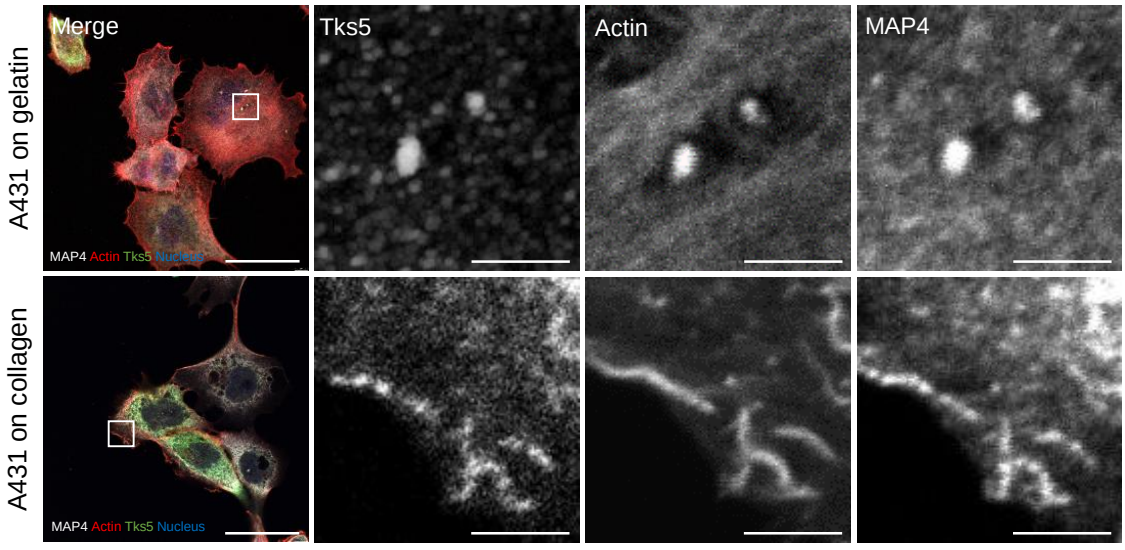

c

Translation	BZW2, EIF3A, EIF4B, FXR1, G3BP1, HNRNPA1, HNRNPAB, IGF2BP2, LARP4, NONO, NUFIP2, PABPC1, PRL36, PTBP1, PUF60, RPL0, RPL3, RPL4, RPL5, RPL6, RPL7, RPL7A, RPL8, RPL10A, RPL13, RPL14, RPL15, RPL18A, RPL19, RPL29, RPL32, RPL34, RPS4X, RPS6, RPS6KA4, RPS8, RRBP1, RTRAF, SPATS2, SRSF1, SSB, STAU1, SYNCRIP, TCOF1, YBX1, YBX3
Actin Cytoskeleton	CALD1, CTTN, EMD, FNBP1L, MYH9,
Adhesion	CD44, ITGA5, PVR
Others	ADAM15, ADAM19, ASPH, BAG3, BASP1, C1QBP, CLTB, DLD, GUSB, HNRNPU, LAMP1, LAMP2, LRRC59, MAP4, MMP14, NPM1, PPM1G, PPP1CA, PRKAA1, PRKAG1, PRR2C2, PRRC2A, PSMD7, RTN4, SART1, STX7, THBD, YWHAB, YWHAE, YWHAG, YWHAH, YWHAQ, YWHAZ

Supp Figure 3: No effect of translation on invadosomes formation.

a

Stylli and *al*, 2009	DDX3X, EEF2, HNRNPK, MetRS, NCL
Thuault and *al*, 2020	EIF2S3, EIF4A3, ELP4, ELP6, EPL5, IGF2BP2, MREAA1
Mallawaaratchy and *al*, 2015	EEIF1E1, KARS1, YBX1
Ezzoukhry and *al*, 2018	ANP32A, BTF3L4, CARS, DDX3X, DDX17, EEF1A2, EEF1D, EEF1G, EEF2, EEFA1A, EFTUD2, EIF2A, EIF2S1, EIF3C, EIF3E, EIF3F, EIF3G, EIF3H, EIF3I, EIF3K, EIF3L, EIF3M, EIF4B, EIF5A, ELAVL1, EPRS, FARSA, FXR1, G3BP1, HNNRPF, HNRNPA1, HNRNPA2B, HNRNPC, HNRNPH1, HNRNPK, HNRNPL, HNRNPM, HSP90B1, HSPA5, IGF2BP1, IGF2BP2, IGF2BP3, KHSRP, MYBBPA1, NONO, PA2G4, PABPC1, PLR35A-PS3, PSMC1, PTBP1, RARS, RBM14, RPL10, RPL10A, RPL12, RPL22, RPL23, RPL23-PS3, RPL26, RPL28, RPL30, RPL31, RPL34, RPL35A, RPL36A, RPL37A, RPS3, RPS4X, RPS11, RPS13, RPS14, RPS15A, RPS16, RPS20, RPS26, RPSA, RRBP1, RSP3A, RSP12, RSP19, SERBP1, SF3A1, SF3B3, SNRPA, SRRT, SYNCRIP, TRIM28, YBX3

b

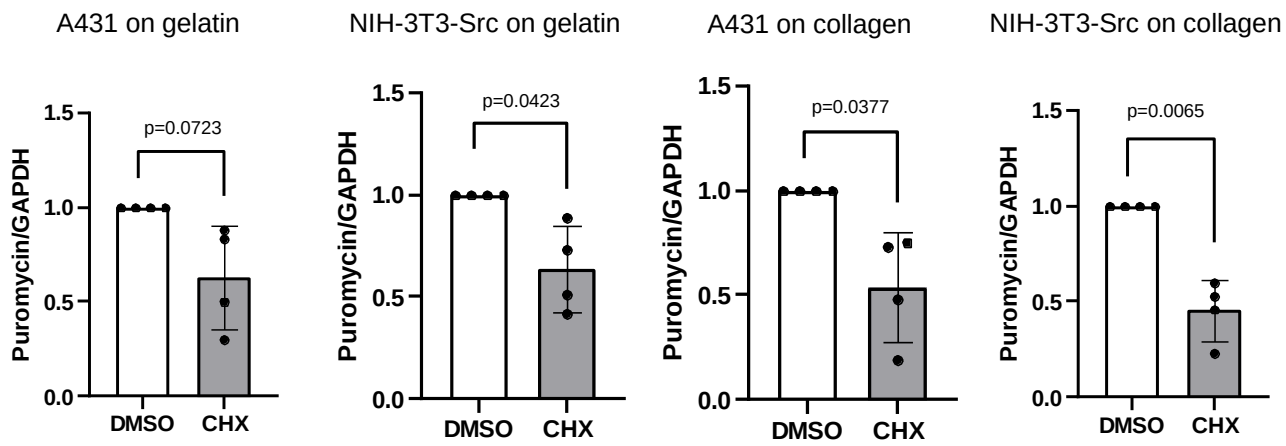

c

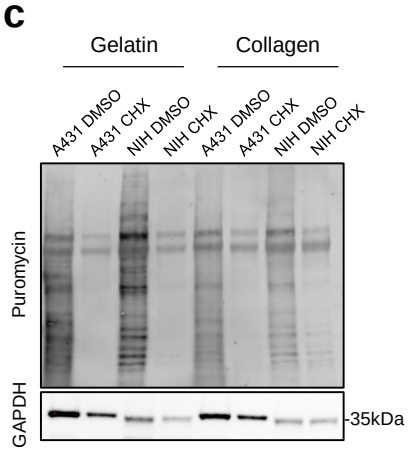

d

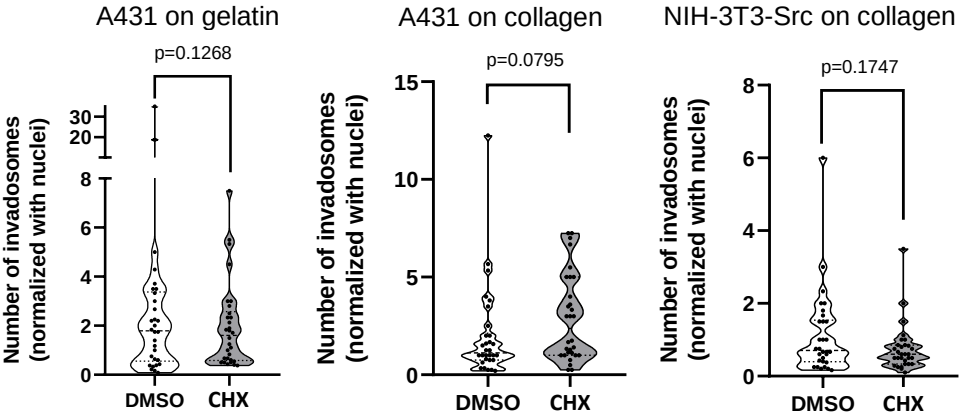

e

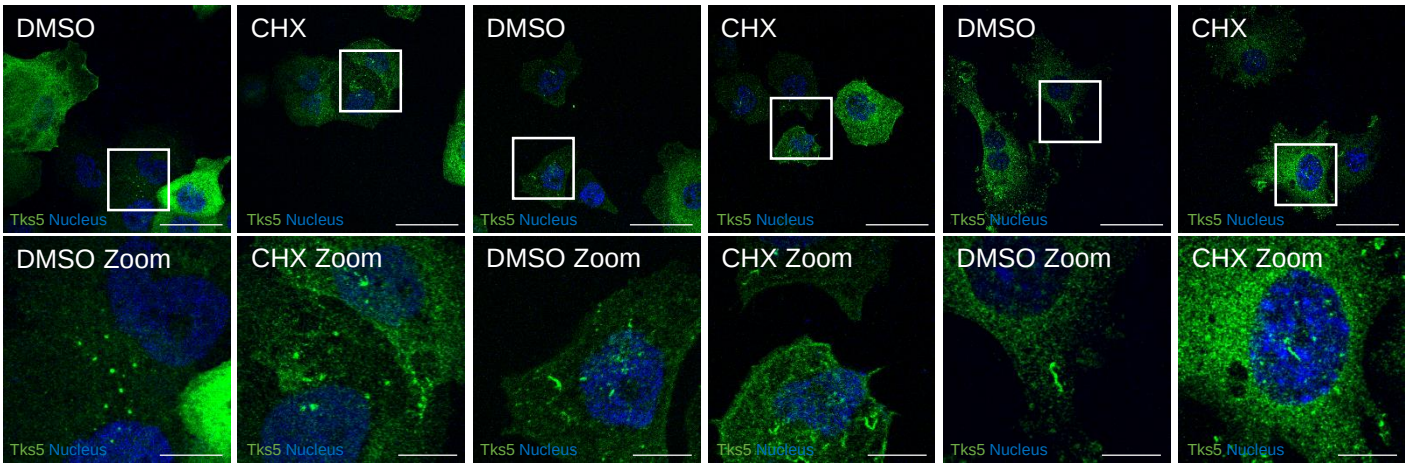

f

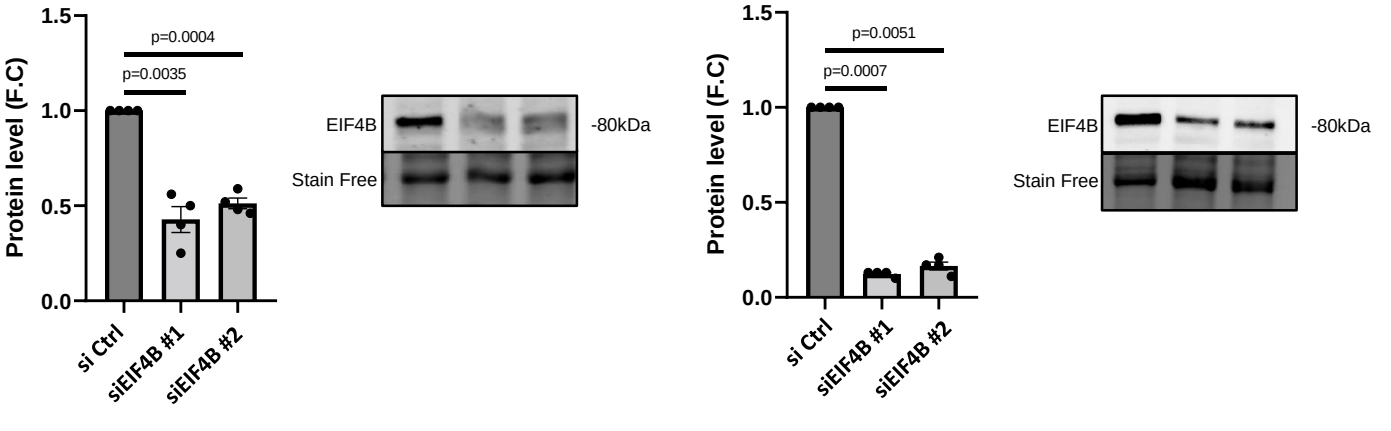

Supplemental table 1 : Summary table of proteins present in invadosomes identified by mass spectrometry analysis of Tks5 interactome

Names	Total	Elements
A431_C A431_P NIH3T3_C NIH3T3_P	88	ADAM15 ADAM19 ASPH BAG3 BASP1 BZW2 C1QBP CALD1 CD44 CLTB CTTN DLD EIF3A EIF4B EMD FNBP1L FXR1 G3BP1 GUSB HNRNPA1 HNRNPAB HNRNPU IGF2BP2 ITGA5 LAMP1 LAMP2 LARP4 LRRC59 MAP4 MMP14 MYH9 NONO NPM1 NUFIP2 PABPC1 PPM1G PPP1CA PRKAA1 PRKAG1 PRRC2A PRRC2C PSMD7 PTBP1 PUF60 PVR RPL3 RPL4 RPL5 RPL6 RPL7 RPL7A RPL8 RPL10A RPL13 RPL14 RPL15 RPL18A RPL19 RPL29 RPL32 RPL34 RPL36 RPLP0 RPS4X RPS6 RPS6KA4 RPS8 RRBP1 RTN4 RTRAF SART1 SH3PXD2A SPATS2 SRSF1 SSB STAU1 STX7 SYNCRIP TCOF1 THBD YBX1 YBX3 YWHAB YWHAE YWHAG YWHAH YWHAQ YWHAZ
A431_P NIH3T3_C NIH3T3_P	29	ALYREF BCAP31 CAV2 CCDC47 CD9 CHMP4B DLST DNAJC5 FUBP1 FUS GOLM1 HPRT1 ITGA3 LASP1 MANF NACA NHERF1 PCNP PPP1CB PPP1R12A PRDX3 PRKCSH RCN1 RCN3 RPS17 SNAP23 SOD2 SRSF5 ZRANB2
A431_C NIH3T3_C NIH3T3_P	6	CLTA EEA1 EIF3C P4HB SMNDC1 SRSF2
A431_C A431_P NIH3T3_P	84	ACSL4 AIFM1 AP2A1 AP2A2 AP2B1 AP2M1 ARHGEF40 CAPRIN1 CCDC86 CD47 CELF1 CKAP4 CSDE1 DARS1 DDX1 DDX5 DDX17 DHX15 EBNA1BP2 EIF2S1 EIF3H EIF4A3 EIF4E EXOSC9 FAU FBXO3 FGD1 FLNB FXR2 GTPBP4 H1-0 HNRNPA0 HNRNPH1 HNRNPM HNRNPUL1 IGF2BP3 ILF2 KHDRBS1 KRT6A LARP1 LARS1 MIB1 MOGS MRTO4 MYL6 MYO1E MYOF NCBP1 NIPSNAP2 NSDHL PABPC4 PAK1IP1 PCDH1 PRKAB1 PRKRA PURA PURB QARS1 RBM17 RCC2 RFC4 RPL12 RPL22 RPL28 RPL30 RPL35A RPL37A RPS3A RPS11 RPS12 RPS19 RPS26 RPS27 SEC63 SFPQ SLC25A13 SMC4 SNRPA1 SQOR TARDBP TMOD3 U2AF2 UPF1 ZC3HAV1
A431_C A431_P NIH3T3_C	36	ACOT9 ATXN2L BSG CALR CCT2 CDK1 CS CYB5R3 CYCS EIF4G1 ERO1A H1-5 HNRNPA2B1 HSD17B10 HSD17B12 HYOU1 KTN1 LGALS3 LUZP1 MAP7D1 MSN MTDH NPTN RAB11FIP1 RPL18 RPS2 SEPTIN2 SEPTIN9 SERPINH1 SF3B2 SH3KBP1 TFG TOR1AIP1 TPM1 TTC1 ZC3H15
NIH3T3_C NIH3T3_P	92	ACIN1 ACP2 ALCAM ANP32A APOBR ARGLU1 ARID1A ARPC4 BCLAF1 BIN1 BRI3BP BTF3 CAST CCDC9 CCDC124 CD63 CD81 CDH2 COLEC12 CSTF2 DBN1 DBNL DDX46 DEK DNAJC8 EEF1B EIF4H ELOB EMB EPB41L2 FKBP3 FKBP10 FXYD5 GM45713 GSR GTF2F1 H1-2 HDGF HDGFL2 HMBS HSPE1 IGF2BP1 IWS1 LGALS1 LRPAP1 MAGEA13 MAP1A MARCKS MXRA7 NES NOLC1 NPC2 NUCB1 NUCKS1 NUP50 PACSIN2 PAKAP PEX19 PGRMC1 PGRMC2 PHACTR4 PLIN3 PMF1 PPP1R18 PPP4R2 PTGES RAB11FIP5 REEP5 RHOC RPL10L RPL17 RTN3 S100A11 SARNP SGTA SIRPA SLC2A1 SNAP29 SOD1 SPARC SRSF7 THRAP3 TP53BP1 TPBG TPR TSPAN3 TXN UBAP2 UBAP2L UBQLN4 VTI1B WASHC2
A431_P NIH3T3_P	32	CDK11B CFL1 CSNK2B DDX56 DKC1 ELAVL1 G3BP2 GRB2 GRPEL1 H1-4 HP1BP3 LEMD2 NAT10 NOC4L NUDT21 OCIAD1 PRC1 PSMB2 RAB10 RAB21 RALB RPL23A RPLP2 RPS5 RPS7 RPS14 RPS20 RPS28 RRP1 RTCA SF1 UTP14A
A431_C NIH3T3_P	11	ESYT2 FMR1 GOT2 KRT16 MAN2A1 PDCD10 PSME2 RPS15A SNRPB2 SQSTM1 SRRT
A431_P NIH3T3_C	31	CALU CAPZB CDV3 CLINT1 CNPY3 DDRGK1 EFHD2 EWSR1 HNRNPA3 LNPEP MAPRE1 MYH10 NUCB2 NUDC PAWR PEX14 PFN1 PSAP PSME1 RAD23B RANGAP1 RPS24 SCAMP1 SERBP1 SERPINC1 SLC44A1 SNX1 STX4 STX12 TPM4 TWF1
A431_C NIH3T3_C	10	ARFGAP1 COL1A1 ECE1 FAM177A1 HADH KRT1 PCYOX1 PDLIM5 PLXNB2 SCP2
A431_C A431_P	587	AAAS ABCF1 ABHD10 ABI1 ABO ACAD9 ACADVL ACBD3 ACOT8 ACSL3 ACTBL2 ACTG1 ACTN1 ACTN4 ACTR2 ACTR3 ADAM10 ADAMTSL4 ADAR ADPGK AFAP1L2 AGK AHCYL1 AIFM2 AIMP1 AIMP2 AK2 AKAP12 ALDH1A3 ALDH3A2 AMY1A ANXA1 APMAP ARAF ARCN1 ARHGAP1 ARHGEF2 ARL6IP5 ARPC2 ASAH1 ASCC1 ASCC2 ASCC3 ATAD3A ATL3 ATP1A1 ATP2A2 ATP2B4 ATP5F1A ATP5F1C ATXN10 BAG4 BAIAP2L1 BCL2L13 BUB3 BYSL C1orf226 C6orf132 C7orf50 C8orf33 CAD CAND1 CANX CAPN1 CAPZA1 CAPZA2 CAVIN1 CAVIN3 CBLB CCNK CCT3 CCT4 CCT6A CCT7 CCT8 CD82 CDC5L CDC42EP1 CDCP1 CDH1 CDH3 CDK9 CDK13 CENPB CEP170B CGAS CHCHD2 CKAP5 CKMT1A CLP1 CLTC CMAS CNP COL17A1 COLGALT1 COPA COPB2 COPE COPG1 CORO1C CPNE1 CPOX CPSF6 CPSF7 CPT1A CRYBG1 CSNK1A1 CSNK2A1 CTNNA1 CTNNB1 CTNND1 CTPS1 CTSB CTSD CUL7 CYB5R1 CYFIP1 CYP2S1 DAP3 DAPK3 DCAF5 DDB1 DDOST DDX3X DDX6 DDX21 DDX24 DDX39B DDX47 DDX55 DDX60 DECR1 DHCR24 DHRS7 DHX9 DHX30 DHX36 DHX57 DIMT1 DNAJA2 DNAJA3 DNAJB12 DNAJC13 DTX3L ECH1 EDC4 EEF2 EGFR EHD2 EHD4 EIF2AK2 EIF2S2 EIF2S3 EIF3B EIF3E EIF3F EIF3G EIF3J EIF4A1 EIF4A2 EIF4G2 ELAVL2 EMC1 EMC2 EPHA2 EPRS1 ERBIN ERGIC1 ERGIC3 ERMP1 ERP29 ERP44 ESRP1 ESYT1 EXOSC2 EXOSC5 EXOSC10 F11R FAF2 FAM3C FAM83A FAM91A1 FAM98A FAM98B FAM120A FAR1 FBXO22 FH FHL2 FHL3 FIP1L1 FLII FLNA FLOT1 FNBP1 FNDC3B GAA GALNT2 GALNT3 GANAB GBA1 GEMIN4 GET3 GIPC1 GLG1 GLS GMPS GNL3 GNL3L GOLGA2 GOLGA4 GPD2 GRB7 GRSF1 GRWD1 GSN GTF3C2 H1-10 HACD3 HADHA HADHB HARS1 HDAC6 HECTD1 HELZ2 HLA-A HLA-B HMOX2 HNRNPC HNRNPD HNRNPF HNRNPK HNRNPR HNRNPUL2 HSD17B4 HSDL2 HSP90B1 HSPA1B HSPA2 HSPA5 HSPA8 HSPB1 HSPH1 IARS1 ICAM1 IDH3B IFI16 IKBIP ILF3 INF2 INPP5K IPO5 IQGAP1 ISG20L2 ITCH ITGA2 ITGAV ITGB6 IVL KARS1 KCTD12 KIAA0930 KIAA1522 KIF2A KPNB1 KRT6B KRT8 KRT17 KRT18 L1RE1 LACTB LAMA3 LAMB3 LAMC2 LANCL2 LCN2 LETM1 LGALS3BP LIMA1 LMAN1 LMAN2 LPCAT2 LRPPRC LRRC1 LRRC8A LSG1 LSR LUC7L2 MACF1 MAGEA4 MAGED2 MAN1B1 MAOA MAP7 MARK2 MARS1 MAVS MBOAT7 MCM5 MDH2 MFAP1 MICAL2 MIOS MLEC MORC2 MOV10 MRPL4 MRPS2 MRPS5 MRPS7 MRPS9 MRPS18B MRPS22 MRPS27 MRPS31 MRPS35 MSH2 MSH6 MTHFD1L MTHFD2 MTPAP MTREX MVP MX1 MYCBP2 MYO1B MYO1C MYO1D MYO5A MYO5B MYO6 NAGK NAP1L1 NCEH1 NCKAP1 NCL NCLN NCSTN NDRG1 NECTIN4 NIT2 NKRF NMNAT1 NOMO1 NOP2 NRDC NSUN2 OAS2 OAS3 OASL OAT OPA1 OSBPL8 OTUB1 P4HA2 PA2G4 PACSIN3 PARP1 PARP9 PARP12 PARS2 PBXIP1 PC PCBP2 PCYT1A PDIA3 PDIA4 PDIA5 PES1 PFKM PFKP PHLDA1 PIP5K1A PISD PKP3 PLBD2 PLEKHA5 PLOD1 PLOD2 PLOD3 PLRG1 PLSCR1 PML POLRMT PON2 POP1 POR PPFIA1 PPFIBP1 PPIB PPP2CA PPP2R1A PRKAB2 PRKAG2 PRKDC PRMT1 PRMT5 PRPF3 PRPF19 PSMA4 PSMC2 PSMC5 PSMD2 PSMD3 PSMD8 PSMD11 PTCD3 PTDSS1 PTGES2 PTGS1 PTPN1 PTPN6 PWP1 QSOX1 RAB3GAP1 RAB3GAP2 RACK1 RAE1 RARS1 RASAL2 RBM4 RBM14 RBM28 RBM39 RCL1 RDH11 RECQL RETSAT RFC2 RFC3 RFC5 RHOT2 RIOX2 RNH1 RPL9 RPL10 RPL11 RPL13A RPL17-C18orf32 RPL21 RPL23 RPL24 RPL26 RPL27 RPL27A RPL31 RPL35 RPN1 RPN2 RPS3 RPS9 RPS13 RPS16 RPS18 RPS23 RPS25 RPSA RTCB SART3 SCAMP2 SCARB2 SCFD1 SCRIB SDC4 SDHA SEC16A SEC23A SEC23B SEC24C SEC61A1 SEMA3C SERPINB1 SERPINB2 SERPINE1 SFN SGPL1 SH3BP4 SHMT2 SLC3A2 SLC7A5 SLC16A3 SLC25A22 SLC25A24 SLC27A4 SLFN5 SMAD3 SMC1A SND1 SNX9 SPATS2L SPINT1 SPOCD1 SPTAN1 SPTBN1 SPTLC1 SPTLC2 SRP54 SRP68 SRPK1 SRPRA SRPRB SRRM2 STAU2 STIM1 STOM STRAP SUMF2 SUPT16H SVIL TACSTD2 TAP1 TAPBP TARS2 TBL2 TCP1 TFAM TFB1M TFB2M TFRC TGFBI THBS1 THSD4 TIMM44 TIMM50 TJP1 TM9SF2 TM9SF4 TMCC3 TMEM43 TMPO TMTC3 TNFAIP2 TNKS1BP1 TOE1 TOP1 TOR4A TRABD TRAF7 TRAM1 TRAP1 TRIM25 TRIM28 TRIM32 TRIM56 TRIP4 TRIP10 TRMT1L TRMT2A TRMT6 TRMT10C TSPYL1 TUBB6 TUFM TUT7 U2SURP UBR4 UBTF UGGT1 UQCRC2 USP7 USP9X USP15 USP34 VAPA VAPB VAT1 VCP VDAC3 VPS26A WASL WDR1 WDR5 WDR12 WDR26 WDR82 WIPF2 XPO1 XRCC5 XRCC6 XRN1 XRN2 YTHDC2 YTHDF2 ZC3H18 ZFPL1 ZMPSTE24 ZNF385A
NIH3T3_P	135	36951 5031439G07RIK ABCB1B AFG3L1 AGO3 AK1 ANAPC1 API5 AQP1 ARF2 ARF4 ARL1 ATAD1 ATP5PB AURKB BAG2 BLVRB CAMK1 CAMK2D CBX3 CD2BP2 CDC40 CDK6 CHD4 CIAPIN1 CISD2 CNPY2 CPSF1 CSTF3 CTDSPL2 CYB5B DCAF13 DNMT1 EIF1A EIF2S3X EIF5A FAM32A GLYR1 GM20521 GNS GSTO1 HDAC1 HDAC2 HINT1 HIRIP3 HMGA2 HS2ST1 IAP IFI202 IFITM3 KPNA2 KPNA6 LAMC1 LMNB2 MACROH2A2 MRPL12 MSI2 MTA2 MYADM MYBBP1A MYEF2 NDUFV1 NFU1 NGDN NOTCH2 NRD1 NUP93 NUP107 NUP160 OTUD4 PAFAH1B3 PCM1 PDLIM7 PGAM5 PHC2 PNO1 POLR2E PRDX6 PRKAR2B PRPF4 PRPF6 PRPF31 PRPF40A PRPSAP1 PSMA2 PTBP2 PTPRE RAB1A RAB1B RAB5A RAB5C RAB6A RAB7A RAB11B RAB14 RAC1 RAD21 RALA RANBP1 RBM19 RBMS1 RDH13 RPA1 RRAS2 S100A4 SCML2 SEC22B SH3PXD2B SLC25A4 SLC25A10 SLC29A1 SLC44A2 SLTM SMARCC2 SMARCE1 SMCHD1 SNRNP40 SNRPA SRSF3 ST13 STAG1 STEAP3 STMN1 SYNE3 TMED9 TMED10 TMX1 UBE2L3 UBXN4 UTP3 UTP6 WDR33 YTHDF3 ZFAND6 ZFR
NIH3T3_C	142	2900026A02RIK 8030462N17RIK ACADL AFDN AHNAK2 AK4 ALAD ANLN ANP32E ANXA5 APOA1 ATF7IP ATXN2 BOD1L BSDC1 CAV1 CAVIN2 CCDC50 CD2AP CD34 CD151 CD200 CDC37 CEP170 CFDP1 CNPY4 COBLL1 COL1A2 CRELD2 CSF1 D17H6S53E DAD1 DAG1 DHODH DIDO1 EEF1D EFCAB14 EHD1 EIF3J2 EIF5B EPB41L3 FKBP7 FKBP9 FSTL1 FTL1 FTSJ3 GOLGA5 GOLIM4 GOLT1B GOT1 GRN HAL HEXIM1 HMGN5 HSPA13 IDI1 IRF2BP2 ITGB1 JPT2 KCNAB2 KCT2 KRT76 KRT78 LIG1 LRRFIP1 LRRFIP2 LSM14A LSS LTBP1 LTBP3 MAP1B MAP6 MARCKSL1 MCL1 MDC1 MIX23 NECTIN1 NECTIN3 NRADD NSFL1C PALM PARK7 PDAP1 PDLIM1 PDPN PGAM1 PGM1 PLAUR PLP2 PPP1R7 PPP1R11 PRRC2B PSIP1 PSMD4 PSME3 PTTG1IP PYM1 RABL6 RAD23A RAET1A RANBP3 RPIA RPS21 RSU1 RWDD1 SAFB2 SCPEP1 SEPTIN11 SERPINB6A SERPINF1 SF3B1 SFR1 SGSH SLC12A2 SNW1 SOX9 SPECC1 SPP1 SSR1 STX8 SUPT5H TACC2 TALDO1 TEX101 TGOLN2 TNFRSF10B TPD52L2 TPM3 TSPAN6 TTN TXNDC15 UBQLN1 UBQLN2 ULBP1 USO1 VAMP3 VKORC1L1 VPS26B VSIG10 VTI1A WIPF1 YIPF3
A431_P	262	ABCD3 AGTRAP AJUBA ALDH18A1 ANKLE2 ANXA8 APOBEC3B ARPC1A ARPC1B ARPC4-TTLL3 ATP2C1 B2M B3GAT3 BAIAP2 BCAS2 BOP1 BRIX1 CACYBP CALM2 CALML3 CAMK2G CCDC59 CCNT1 CDC42 CERS2 CHCHD3 CNBP COMT COQ9 CRKL CSE1L CSNK1D CYC1 DDX20 DDX27 DDX41 DHCR7 DIABLO DNAJA1 DNAJB2 DNAJB11 DNAJC3 DNAJC10 DNAJC14 DNAJC16 DOCK7 DPM1 DRG1 EEFSEC EIF3CL EIF3I EIF6 ELOA EMC3 EPB41L4B EPPK1 ERCC6 ERLIN2 EXOSC4 EXOSC6 EXOSC7 FARSA FARSB FBL FBXO31 FOSL1 FTH1 FUBP3 GEMIN5 GFPT1 GM2A GNL2 GPAA1 GPI GTF2H2 GTF3C3 GTF3C4 GTF3C5 H2A HBB HCCS hCG_1984214 HDAC10 HK2 HMGB1 HMGB2 HSP90AB4P HTATIP2 HTRA2 HYAL2 IFRD1 IMMT IMP4 IMPDH IPO7 ISG15 ITPRIP KHSRP KIF1C KRR1 KRT13 KRT15 KRT82 LAD1 LARP4B LLGL1 LRCH3 LYAR M6PR MAGT1 MARK3 MATR3 MBNL1 MCAT MFSD10 MGAT1 MPG MPHOSPH10 MPRIP MRM3 MRPL2 MRPL15 MRPL37 MRPL47 MRPS12 MRPS15 MRPS23 MRPS34 MTAP MX2 MYDGF MYH14 MYL12A MYO18A NAP1L4 NAPA NDUFA10 NDUFS2 NFX1 NIPSNAP1 NOP56 NOP58 NOS1AP NSF NSUN4 NSUN5 NTAQ1 NUDT5 NUMB P3H2 PCBP1 PCMTD1 PCNA PEX16 PFKL PIGT PLAA PLAU PLEC PLEKHG3 PNN POLDIP2 POLDIP3 POLR3A PPL PPP1R10 PPP2R2A PPP3CA PPP6C PRDX4 PRDX5 PRKAR2A PRORP PSMA1 PSMB3 PSMC1 PSMC3 PSMC6 PTBP3 PTK7 PTPMT1 PUM3 PYGL RAB5B RAB8B RAB34 RAB38 RAN RBM27 RBM33 RBM47 RCN2 RFC1 RHOT1 RIDA RPP30 RPS15 RRAGB RRP1B RRP12 RTKN RUVBL1 RUVBL2 S100A6 S100A8 SDF2 SEC61B SEC62 SET SETX SF3A1 SFXN3 SIGMAR1 SLC25A3 SLC35B2 SMN1 SNRPB SPOUT1 SPRR1B SPTY2D1 SRP14 SRP72 SSRP1 STT3A STT3B SURF4 TAP2 TBCA TBL3 TECR TEFM TIMP3 TMCC1 TMEM40 TMEM214 TMX3 TOLLIP TOM1L2 TOP3B TOR1AIP2 TPM2 TPP1 TRIM65 TRMT61A TSG101 TSR1 TTC13 TUBB TUBB4B TWNK UFL1 UNC45A USP10 VDAC1 VDAC2 VPS45 WDR3 WDR36 WDR77 YTHDF1 Z02 ZNF598
A431_C	119	ABCB7 ABHD12 ACOT7 AFAP1 AFG3L2 AGO2 AHCY AHSA1 AK4P3 ANXA8L1 ARFIP1 ATL2 ATP1B1 ATP1B3 ATP5MF-PTCD1 ATP6AP1 BZW1 CAPG CAPN2 CASP14 CAT CCN1 CD46 CHERP CLPX COPB1 CSTA DEFA1 DHX37 DSC3 DSP DYNC1H1 ECHS1 ECM1 EIF2B4 EIF3L EIF5 ERAL1 ERAP1 ERLEC1 ETFA ETFB ETHE1 FAM20B FLG FMNL3 FN1 GARS1 GFM1 GIGYF2 GLUD1 H1-3 HDLBP HEXB HM13 HMGCL HSP90AB1 HSPA4 HSPBP1 HSPD1 IDH2 IGHA1 IGKC JUP KPRP KRT80 LBR LCLAT1 LMAN2L LYZ MAPK1 MCM3 MFN1 MRPL44 NDUFA4 NECTIN2 NFKB2 NUDCD1 NUP155 P4HA1 PIGK PIGS PPT1 PROSER2 PRPS1 PSMB8 PSMD1 PSMD6 PSMD13 PSMD14 PTGFRN PUM1 PUS1 PYCR1 RNF213 S100A14 SACM1L SAMD9 SEC23IP SEPTIN8 SERPINB6 SLC38A5 SMC2 SPRYD3 STK24 STX6 SUCLG2 TBL1XR1 TMEM87A TOMM70 TYMP UBA1 UCHL5 UFD1 UMPS VPS4A VPS35 YARS2 ZG16B

Supplemental table 2 : Summary table of crossed data obtained by mass spectrometry for the rosettes with the data from Ezzoukhry and *al.* paper

Proteins commonly identified in rosettes in Tks5 immunoprecipitation experiment and Ezzoukhry et al. paper
ANP32A, ARPC4, BAG3, CALD1, CAMK2D, CAPRIN1, CHMP4B, CKAP4, CLTA, CTTN, DDX17, DLST, EIF2S1, EIF3C, EIF3H, EIF4B, EIF5A, ELAVL1, FLNB, FUBP1, FXR1, G3BP1, GRPEL1, HNRNPA1, HNRNPH1, HNRNPM, HSPE1, IGF2BP1, IGF2BP2, IGF2BP3, KPNA2, LASP1, MAP4, MYBBP1A, MYEF2, MYH9, MYL6, MYOF, NACA, NONO, NPM1, PABPC1, PABPC4, PPP1CA, PRDX3, PSMA2, PTBP1, PURB, RAB5C, RAB14, RAB21, RPL10A, RPL12, RPL22, RPL23A, RPL28, RPL30, RPL34, RPL35A, RPL37A, RPS3A, RPS4X, RPS11, RPS12, RPS14, RPS15A, RPS19, RPS20, RPS26, RPS27, RRBP1, SFPQ, SNRPA, SRRT, STMN1, SYNCRIP, TARDBP, YBX3

Translation proteins highlighted in red in the table